UiT
THE ARCTIC
UNIVERSITY
OF NORWAY

Faculty of Science and Technology

Department of Geosciences

Investigating the variability of Atlantic water inflow to the southwestern Barents Sea through Bjørnøyrenna during the Late Glacial and Holocene based on benthic foraminifera and sediment properties.

—

Anders Tysnes

Master's thesis in marine geology and geophysics GEO-3900
May 2017

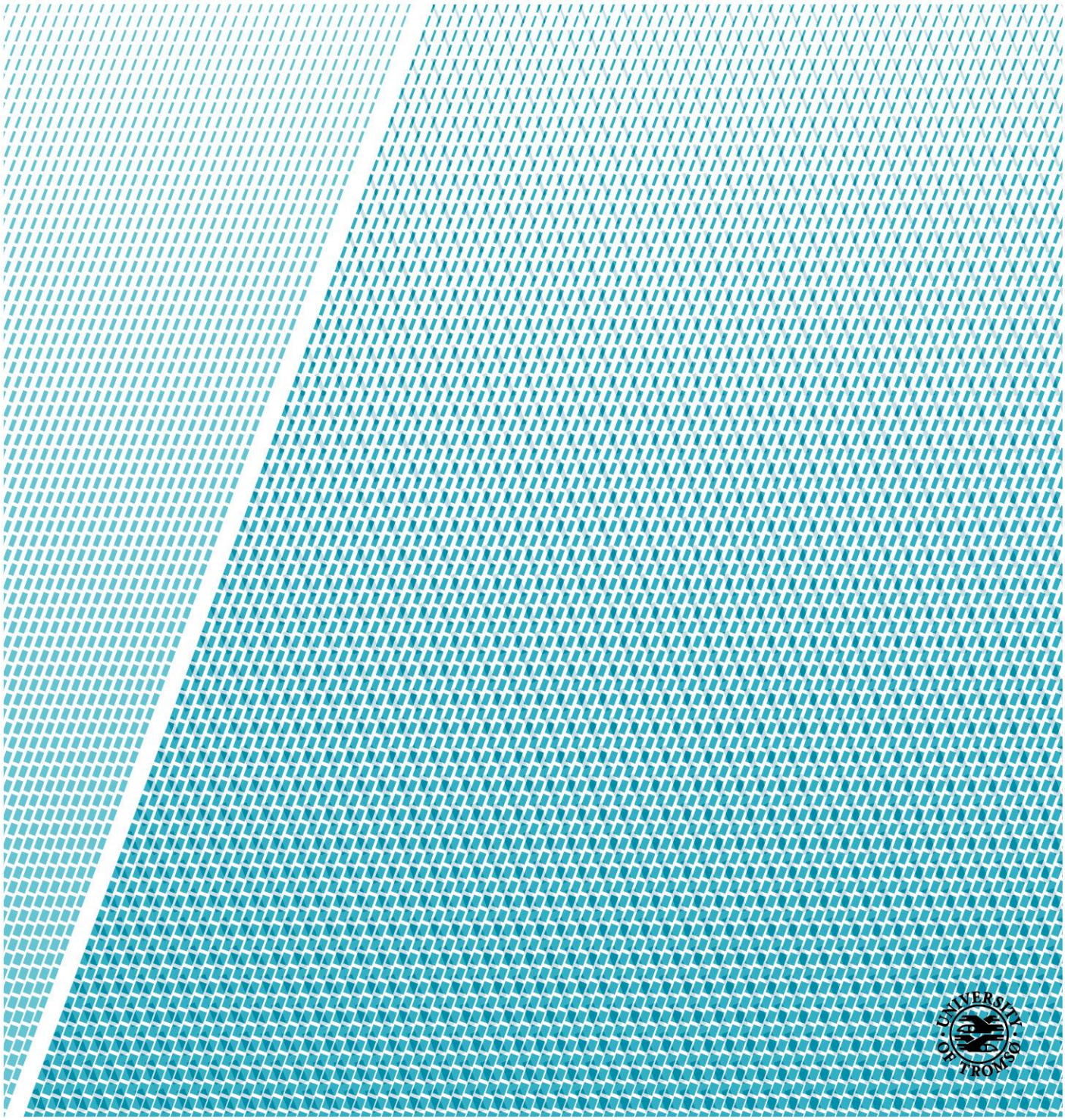

Abstract

This study is a part of the Barents Sea drill cuttings research initiative (BARCUT), investigating the inflow of Atlantic water to the southwestern Barents Sea during the Late Glacial and Holocene as well as providing data for future references.

Five cores, HH12-903-mc, HH12-902-mc, HH12-897-mc, HH12-893-mc and IG15-993-mc, from the southwestern Barents Sea were used to investigate the inflow of Atlantic water to the southwestern Barents Sea through Bjørnøyrenna. The main method used is analyzing benthic foraminifera and the faunal composition, but total organic carbon (TOC), sortable silt mean grain size and grain size distribution are used as supporting data.

The samples were sieved using mesh sizes of 1mm, 100mμ and 63mμ, but only the 100mμ-1mm fraction was used for the foraminiferal analysis. Samples from the top and bottom of the cores were sent to ^{14}C dating to establish a timeframe. For the purpose of this thesis, four time intervals are selected for investigation, representing the Late Glacial (15 500-14 900yr BP), early Holocene (10 900-7300yr BP), mid Holocene (7300-2500yr BP) and late Holocene (2500-400yr BP).

Signs of inflowing Atlantic water are first observed in the Late Glacial. However, it is possible that the core covering this time is partly reworked and thus care should be taken when interpreting the core. Atlantic water is present in the southwestern Barents Sea during the Holocene with varying inflowing strength and influence. The general warming and higher current strength throughout the early Holocene is due to increased inflow of Atlantic water. The currents calms and the Atlantic water flowing in to Bjørnøyrenna are cooler during the mid Holocene compared to the early Holocene. In the beginning of the late Holocene, a marginal ice zone (MIZ) is likely present in the studied area and a more vigorous environment occurs. During the late Holocene, the vigorous environment calms and by the end of the period only a weak current flows over the area, possibly influenced by a seasonal sea ice cover.

Acknowledgements

I would like to thank my supervisors Juho Junttila and Noortje Dijkstra for good guidance and help while working in the laboratory, identifying foraminifera and analyzing the samples. They have also guided me in the right direction during the writing process of my thesis. It was very helpful knowing they had an open office policy, fast and helpful replies to my email and good answers to my questions. I would also like to thank Steffen Aagaard-Sørensen who helped me in the initial phase, getting started with the laboratory work and proofreading my thesis.

Further, I would like to thank the cruise members who gathered the cores and made this thesis possible. I also want to thank Karina Monsen, Trine Dahl and Ingvild Hald, who work in the geology lab at UiT, for always providing help and guidance when asked.

List of Tables

Table 1: Characteristics of the main and local water masses in the Barents Sea, T=temperature in °C, S=salinity. Table from Loeng (1991). 5

Table 2: Core information gathered from the cruise reports. 19

Table 3: Statistical formulas used by GRADISTAT 8.0 to calculate the geometric methods of moments. f=frequency in percent, m=mid-point of interval in metric or phi intervals. Table from GRADISTAT 8.0 28

Table 4: Results from the AMS ^{14}C dating. Cal age = Calibrated age in years before present (yr BP). The 1σ results show the interval in which the true age is 68.3% likely to lie. The 2σ results show the interval in which the true age is 95.4% likely to lie. The extrapolated ages are based on the median probability age. 32

List of figures

Figure 1: A) An overview of the study area. ESC = East Spitsbergen Current, BIC = Bear Island Current, NCaC = North Cape Current, NCC = Norwegian Coastal current and NAC = North Atlantic Current. B) Close up of study area. The core locations are indicated with red dots. Figure modified from Dijkstra et al. (2016). 3

Figure 2: Bathymetric map of the Barents and Kara Seas (Byrd polar research Center, 2001). 4

Figure 3: Ocean currents in the Barents Sea today. WSC=West Spitsbergen Current, NCaC= North Cape Current, NCC=Norwegian Coastal Current. Figure modified from Kartverket. 6

Figure 4: Illustration of transport mechanisms and the grain size they are able to transport to the seafloor. Figure from Gilbert (1990) 8

Figure 5: The extent of the last glacial maximum (LGM) about 20 000yr BP. Sea level is lowered by 120m everywhere. Ice-dammed lakes are shown inside the LGM limit (Mangerud, et al., 2004). 9

Figure 6: The tubes with sample material reacting with hydrogen peroxide, removing organic material. 26

Figure 7: The Udden-Wentworth size scale. Figure retrieved from GRADISTAT 8.0. 27

Figure 8: Core age, in cal yr BP, and average sedimentation rate (cm/ka) plotted against the southwest-northeast position of the cores. The top and bottom depth of the cores are given in the figure. 31

Figure 9: Amount of material >1mm found when sieving. For cores 902 and 903 it mostly consists of organic material. 33

Figure 10: Measured sand content (%) plotted against the measured sortable silt (μm). A linear regression line based on the data points is shown in the figure, from core 993. 37

Figure 11: A and B shows the connection between sand (%), ΔSS and the measured SS in core 993. C shows the measured SS and the SSpot. D shows the current sorted fraction of the sortable silt mean grain size in core 993 37

Figure 12: Grain size, TOC and sortable silt results. 40

Figure 13: Abundance, relative to the entire faunal composition, in percent, of Cribrostomoides spp. and Reophax spp. in core 993. 41

Figure 14: Abundance, relative to the entire faunal composition, in percent, of Cribrostomoides spp. and Reophax spp. in core 893. 41

Figure 15: Abundance, relative to the entire faunal composition, in percent, of Cribrostomoides spp. and Reophax spp. in core 897. 42

Figure 16: Abundance, relative to the entire faunal composition, in percent, of Cribrostomoides spp. and Reophax spp. in core 902. 42

Figure 17: Abundance, relative to the entire faunal composition, in percent, of Cribrostomoides spp. and Reophax spp. in core 903. 42

Figure 18: The total agglutinated flux plotted together with the total calcareous flux to give an impression of their relationship. 43

Figure 19: Overview of the flux of the different species. Note the different x-axis scales. It is assumed a constant sedimentation rate throughout the cores for the flux calculations..... 46

Figure 20: The relative abundance of the ten most common calcareous species for all five cores. Sortable silt (SS), sand, clay, total organic carbon (TOC) and the calcareous flux are shown to the left in the figure. Notice the different x-axis scales. 54

Table of content

Abstract ii
List of Tables vi
List of figures viii
1 Introduction 1
2 Background 3
2.1 Study area 3
2.2 Sediment transport processes 6
2.2.1 Suspension 7
2.2.2 Ice rafted debris 7
2.2.3 Mass movement processes 7
2.3 Deglaciation and the Holocene in southwestern Barents Sea 8
2.3.1 Deglaciation 8
2.3.2 The Holocene 10
2.4 Benthic foraminifera 12
2.5 Ecological preferences 13
2.5.1 *Cribrostomoides* spp. (Cushman, 1910) 13
2.5.2 *Reophax* spp. (Montfort, 1808) 13
2.5.3 *Buccella* spp. (Andersen, 1952) 14
2.5.4 *Cribroelphidium excavatum* (Terquem, 1875) 14
2.5.5 *Cassidulina laevigata* (d'Orbigny, 1826) 15
2.5.6 *Cassidulina neoteretis* (Seidenkrantz, 1995) 15
2.5.7 *Cassidulina reniforme* (Nørvang, 1945) 15
2.5.8 *Islandiella norcrossi* (Cushman, 1933) 16
2.5.9 *Eilohedra nipponica* (Kuwano, 1962) 16
2.5.10 *Lobatula lobatula* (Walker & Jacob, 1798) 16
2.5.11 *Melonis barleeanus* (Williamson, 1858) 17
2.5.12 *Nonionella* spp. (Dawson, 1860) 17
3 Material and methods 19
3.1 Sampling 19
3.2 Freeze drying 19
3.3 Sieving 20
3.4 Foraminiferal analysis 21

3.4.1 Taxonomy notes 22
3.5 Dating 23
3.6 Organic Carbon 24
3.6.1 Sample treatment 24
3.6.2 LECO Analysis 24
3.7 Particle size analysis 25
3.7.1 Sample treatment 25
3.7.2 Sample analysis 26
3.8 Data processing 27
3.8.1 Sortable silt 28
4 Results 31
4.1 Radiocarbon dating 31
4.2 TOC 33
4.3 Grain size and sortable silt 33
4.3.1 HH12-903-mc 34
4.3.2 HH12-902-mc 34
4.3.3 HH12-897-mc 35
4.3.4 HH12-893-mc 35
4.3.5 IG15-993-mc 36
4.4 Agglutinated foraminifera 41
4.5 Calcareous flux 43
4.5.1 HH12-903-mc 43
4.5.2 HH12-902-mc 43
4.5.3 HH12-897-mc 43
4.5.4 HH12-893-mc 44
4.5.5 IG15-993-mc 44
4.6 Calcareous species abundance and flux 47
4.6.1 HH12-903-mc 47
4.6.2 HH12-902-mc 48
4.6.3 HH12-897-mc 49
4.6.4 HH12-893-mc 50
4.6.5 IG15-993-mc 51
5 Discussion 55

5.1 Agglutinated flux 56
5.2 The Late Glacial (15 500-14 900yr BP) 57
5.3 Early Holocene (10 900-7300yr BP) 60
5.4 Mid Holocene (7300-2500yr BP) 62
5.5 Late Holocene (2500-400yr BP) 66
6 Conclusion 73
7 References 75
Appendix 1: Species list 83
Appendix 2: Sample Interval 85

1 Introduction

Warm Atlantic water flowing north, entering the Arctic, is an important source of heat in Arctic region. The variation in the inflow of Atlantic water transported north by the North Atlantic Current (NAC) is believed to affect the climate on land, as it is a part of the thermohaline circulation (Figure 1) (Rahmstorf, 2006; Slubowska-Woldengen, et al., 2008). The Atlantic water brings organic material and contributes to an increase in nutrients to the Arctic, contributing to increased productivity in benthic foraminifera living on the seafloor.

The purpose of this thesis is to investigate the variability of Atlantic water inflow into the southwestern Barents Sea during the Holocene and part of the Late Glacial. Five core sites along the southeastern slope of Bjørnøyrenna are investigated (Figure 1). Using the benthic foraminiferal faunal assemblages, grainsize distribution and the total organic carbon (TOC) concentration, a model illustrating the variability in Atlantic water inflow can be made.

The Barents Sea is an area in the Arctic of special interest due to the economic importance related to potential petroleum activities and fisheries (Saher, et al., 2012). In the later years, a general shift towards temperature tolerant and warm water species is observed in the southwestern Barents Sea (Saher, et al., 2012). The shift towards a warmer climate, regardless of source, is in need of more attention, especially with respect to effects on ecosystems (Saher, et al., 2012). There are relatively few studies from high latitude areas, thus the knowledge of pre-impact conditions are limited (Dijkstra, et al., 2013; Dijkstra, et al., 2015) and this study contributes to increasing our understanding of these conditions.

The climate in southwestern Barents Sea and surrounding areas are sensitive to changes in the inflow of Atlantic water, including temperature change in the ocean, the atmosphere and sea ice conditions (Risebrobakken, et al., 2010). This study will contribute to increased understanding of natural variability and change in transportation patterns of seafloor sediments and foraminiferal response to variations in Atlantic water inflow. This may contribute to an increased knowledge of previous environmental changes and thus contribute to increasing the understanding of the ongoing climate change.

This study is connected to the Barents Sea drill cuttings research initiative (BARCUT) project, and carried out by the Arctic University of Norway in Tromsø (UiT)

The BARCUT project aims to identify environmental impacts of drill cuttings released in to the ocean at the drill sites. BARCUT focus on long-term research and monitoring of petroleum related activities in the Barents Sea region. Eni Norge fully finances the BARCUT project.

This study will provide data on the environmental and climatic conditions of the southwestern Barents Sea during the Late Glacial and Holocene. These data may be used as reference conditions in future studies on impacts of anthropogenic influences in the area as well as providing a model for the variation in Atlantic water inflow during the Late Glacial and Holocene, which may be used in studies constructing models predicting future variations in Atlantic water inflow. In addition, this study can contribute to an improved understanding of the natural environmental variability in the southwestern Barents Sea.

2 Background

2.1 Study area

The area investigated is located in the southwestern Barents Sea, off the north Norwegian coast, at the southeastern edge of Bjørnøyrenna (Figure 1). This is an important area of Atlantic water inflow to the Barents Sea (Loeng, 1991). As the core sites are located at the southeastern edge of Bjørnøyrenna, they are believed to be influenced by the inflow of Atlantic water.

Bjørnøyrenna is one of the largest known submarine troughs along glaciated continental margins. Bjørnøyrenna is influenced by warm Atlantic water flowing north along the continental slope of Norway (NAC) and colder Arctic water flowing south (Figure 1).

There are shallower bank areas on both sides of Bjørnøyrenna. A bank area with depths shallower than 100m is located north of Bjørnøyrenna and a series of troughs and banks are located south of Bjørnøyrenna (Figure 1). Bjørnøyrenna ends in the western part where the continental shelf abruptly ends and the continental slope down to the abyssal plain begins.

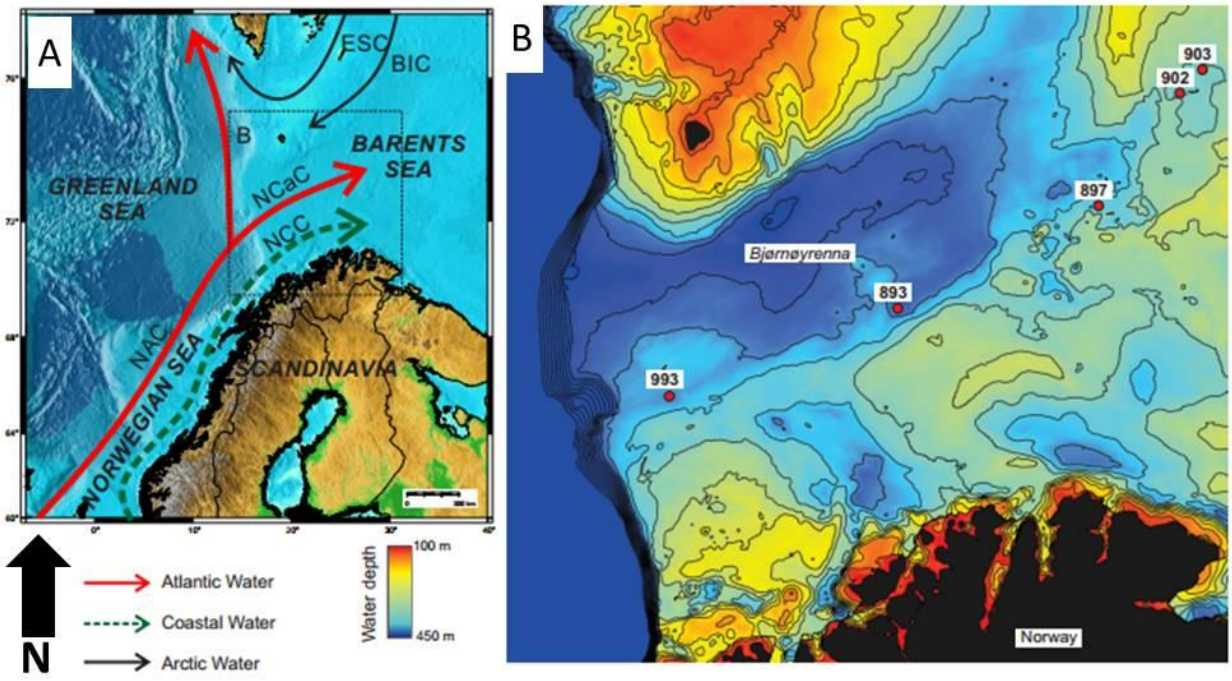

Figure 1: A) An overview of the study area. ESC = East Spitsbergen Current, BIC = Bear Island Current, NCaC = North Cape Current, NCC = Norwegian Coastal current and NAC = North Atlantic Current. B) Close up of study area. The core locations are indicated with red dots. Figure modified from Dijkstra et al. (2016).

The Barents Sea is an epicontinental sea, covering one of the widest continental shelfs on the planet (Figure 2). It is estimated to cover an area of about 1.4 million km^2 (Smedsrud, et al., 2013). The topography of the Barents Sea is relatively uneven with several banks and plateaus separated by troughs. This diverse bottom topography strongly influences the currents. This is especially true for the currents going over some of the bank areas (Loeng, 1991). As the currents are the main transport agent of sediments, the seafloor topography indirectly affects the deposition and transportation of sediments. The Barents Sea is characterized by salinities of 34.3-34.8ppt (parts per thousand) and temperatures below 0°C and is seasonally covered by sea ice (Loeng, 1991).

The vast parts of the Barents Sea are areas of intense heat exchange between the ocean and the atmosphere, mainly driven by the Atlantic water inflow (Risebrobakken, et al., 2010; Smedsrud, et al., 2013). This is especially true during sea ice formation, when a lot of latent heat is released to the atmosphere.

Due to the seafloor topography, the NAC splits into two branches at about 72°N (Figure 3) (Loeng, 1991). One branch continues to follow the Barents Sea slope northwards along the western Svalbard margin into the Arctic Ocean as the West Spitsbergen Current (WSC). The other branch flows into the south Barents Sea as the North Cape Current (NCaC).

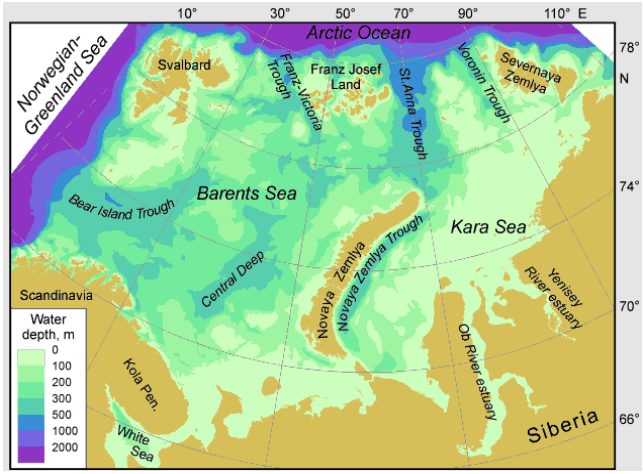

Figure 2: Bathymetric map of the Barents and Kara Seas (Byrd polar research Center, 2001).

The WSC splits into two new branches west of the northern part of Svalbard (Figure 3). One branch continues north around Svalbard as a subsurface current while the other branch turns west and eventually south "recycling" the Atlantic water (Figure 3). The NCaC splits further in to two branches inside Bjørnøyrenna (Figure 3).

The large submarine troughs, separated by shallow bank areas, in the southwestern Barents Sea are a result of several glacial erosion episodes (e.g. Elverhøi et al. (1998)). Bjørnøyrenna and Storfjordrenna are two examples of such large submarine troughs extending in to the southwest Barents Sea continental shelf break. The deepest part of Bjørnøyrenna is found in the western part at depth of approximately 500m. This is also the deepest part of the Barents

Sea, which have an average depth of 230m (Loeng, 1991). The shallow bank areas have a strong impact on currents and act as sediment sources for the deeper parts of the southwestern Barents Sea (Junttila, et al., 2014; Loeng, 1991). Some of the most important banks in the study area are Tromsøflaket, Nordkappbanken, and Sentralbanken.

Three main water masses, Atlantic water, Arctic water and Coastal water, dominate the Barents Sea. Five locally formed water masses are present in addition to the three main water masses defined by their specific properties (Table 1) (Loeng, 1991). Figure 3 illustrates the current patterns in the Barents Sea as they are today.

Names of the water masses		Characteristics of the water masses	
		T,°C	S
Main water masses:			
Coastal Water	(CW)	>2.0	<34.7
(North) Atlantic Water	(NAW)	>3.0	>35.0
Arctic Water	(AW)	<0.0	34.3–34.8
Locally formed water masses:			
Melt Water	(MW)	>0.0	<34.2
Spitsbergenbanken Water	(SBW)	1.0–3.0	<34.4
Bottom Water	(BW)	<−1.5	>35.0
Barents Sea Water	(BSW)	−1.5–2.0	34.7–35.0
Polar Front Water	(PW)	−0.5–2.0	34.8–35.0

Table 1: Characteristics of the main and local water masses in the Barents Sea, T=temperature in °C, S=salinity. Table from Loeng (1991).

The Arctic Front, illustrated with a blue line in Figure 3, is where the Atlantic and Arctic water interact and the Atlantic water is submerged under the Arctic water. The seasonal sea ice edge or marginal ice zone (MIZ) usually follows and defines the Arctic Front during winter and early spring (Loeng, 1991; Hald & Steinsund, 1996; Jennings, et al., 2004).

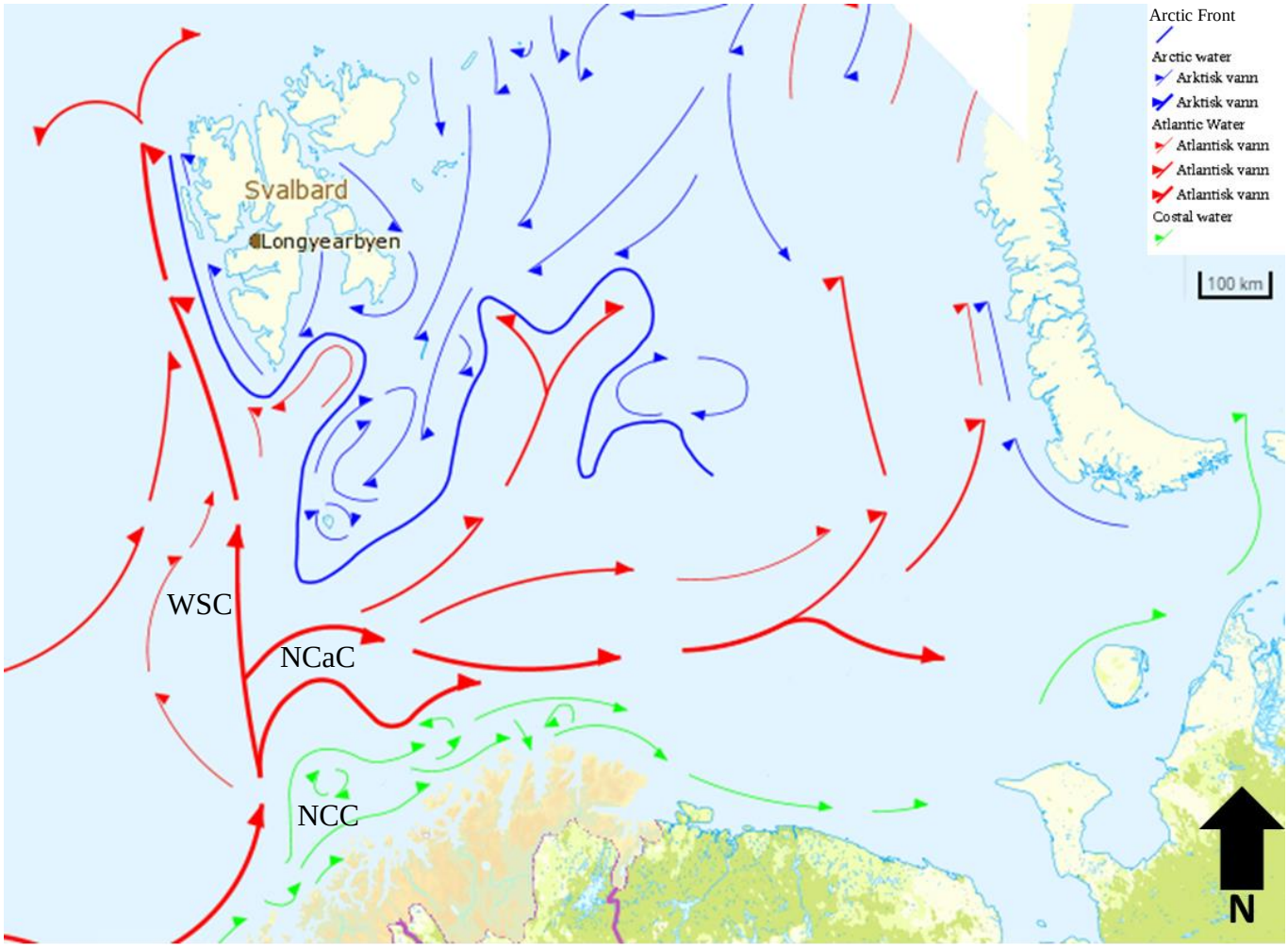

Figure 3: Ocean currents in the Barents Sea today. WSC=West Spitsbergen Current, NCaC= North Cape Current, NCC=Norwegian Coastal Current. Figure modified from Kartverket.

2.2 Sediment transport processes

Several sedimentation processes are and have been active during the Holocene and Late Glacial in the southwestern Barents Sea. All sediment deposited on the sea floor originates from land-based sources and are transported to the deposition area by a variety of processes. Rivers and glaciers erode much of the sediment from mountain areas and transport the material to the ocean. Aeolian processes can transport fine particles out to the oceans. Figure 4 illustrate which grain sizes different transportation mechanisms are able to transport.

Sediments can be reworked after deposition, for example by events like mass movement processes or strong bottom currents (Junttila, et al., 2014; Hass, 2002).

2.2.1 Suspension

Small grainsizes such as clay and silt can be transported long distances in suspension (Figure 4) (Junttila, et al., 2014). As long as the currents maintain a velocity high enough for the particles to remain in suspension, they will not settle. Bottom currents can carry sediment in suspension for long distances. This allows the current strength to be estimated by investigating the sorting of silt grains, called sortable silt. Clay particles tend to flocculate, forming aggregates, not readily interpreted (Hass, 2002).

2.2.2 Ice rafted debris

Ice rafted debris (IRD) occurs in areas with sea ice or icebergs. Sediments trapped in the ice are released and sinks to the seafloor when the ice melts. Icebergs can contain any grain size, from very fine clay particles to large boulders (Figure 4). Larger grains, sand and coarser, are usually assumed to be of ice rafted origin. Icebergs can transport sediments long distances before completely melting away (Gilbert, 1990).

2.2.3 Mass movement processes

Underwater slides and slope failures transport sediment from the shelf to the deep seas. Slopes like the ones on the sides of Bjørnøyrenna may fail, causing reworking of the sediments. Mass movement processes usually occur in areas with high sedimentation rates. Mass movement transport mechanisms are not suppling new sediment to the seafloor, but reworks sediments already present (Ercilla & Casas, 2012). The only exception from this is if the material originates on land and slide in to the ocean by mass movement processes, such as a slope failure in a fjord or at the coast.

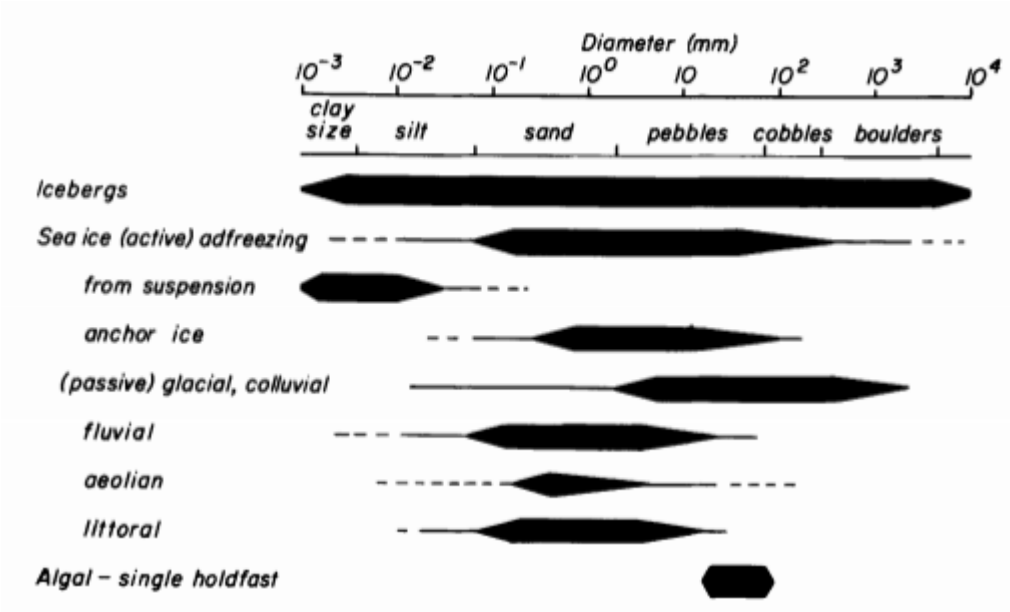

Figure 4: Illustration of transport mechanisms and the grain size they are able to transport to the seafloor. Figure from Gilbert (1990)

2.3 Deglaciation and the Holocene in southwestern Barents Sea

2.3.1 Deglaciation

Grounded ice has at several occasions, covered the Barents Sea throughout the late Cenozoic era (Vorren, et al., 1988a). These glaciations eroded and shaped the Barents Sea bathymetry to what is present today. About 20 000 years before present (1950) (yr BP) the Barents Svalbard Ice Sheet (BSIS) was at its greatest extent in the late Weichselian ice age, commonly known as the last glacial maximum (LGM). At this time, the grounded ice covered a large area including the Barents Sea, Fennoscandia and south to the present Great Britain (Figure 5).

The deglaciation after the LGM in the southwestern Barents Sea occurred stepwise and began about 15 000yr BP (Landvik, et al., 1998). A minimum and maximum age for the onset of the deglaciation is estimated to be 13 700yr BP and 16 200yr BP respectively (Vorren, et al., 1988b)

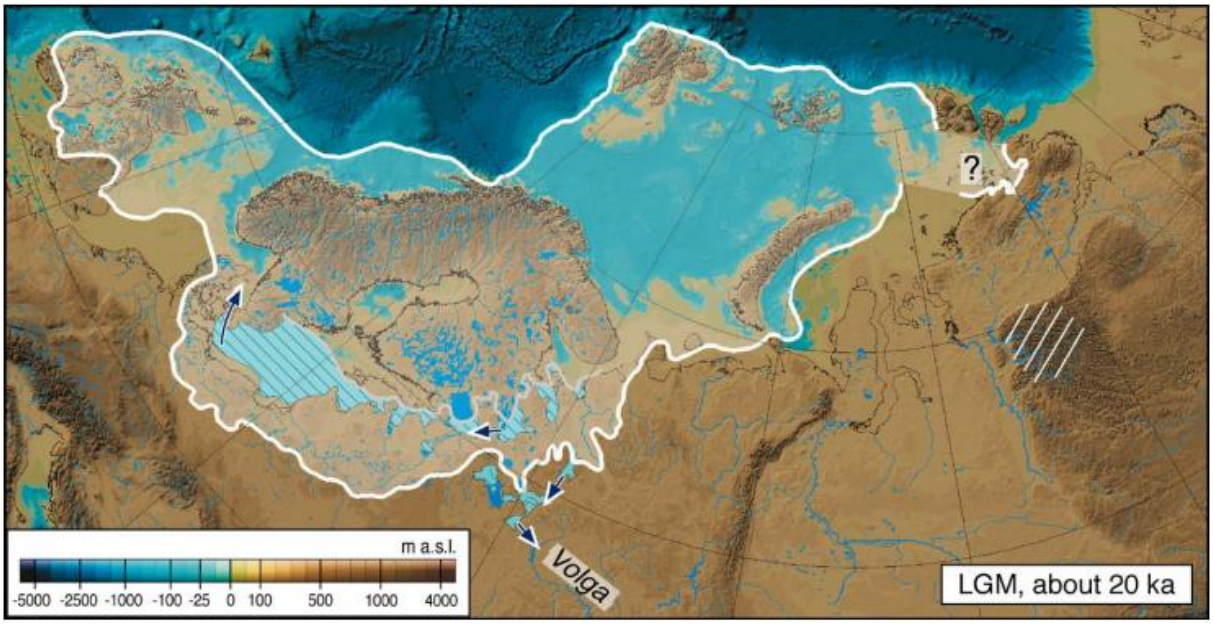

Figure 5: The extent of the last glacial maximum (LGM) about 20 000yr BP. Sea level is lowered by 120m everywhere. Ice-dammed lakes are shown inside the LGM limit (Mangerud, et al., 2004).

Slubowska-Woldengen et al. (2008) suggest that the earliest signs of subsurface inflow of Atlantic water after the last glacial maximum (LGM) can be observed in foraminiferal assemblages on the northern Iceland shelf about 16 000yr BP. The strong Atlantic water signal could be due to the location of Iceland, far from the mainland ice sheets, making it less affected by meltwater (Slubowska-Woldengen, et al., 2008). Junttila et al. (2010) observed indications of Atlantic water inflow to the southwestern Barents Sea 18 700yr BP.

The period 16 000-15 000yr BP is characterized by the presence of benthic foraminifera species associated with cold, low salinity water along the continental margins of the Nordic and Barents Seas (Slubowska-Woldengen, et al., 2008). High content of ice rafted debris (IRD) observed in the northern parts of the North Sea by Klitgaard-Kristensen, et al. (2001), indicating presence of icebergs. Signs indicating the start of the deglaciation close to the north Norwegian mainland are dated to ~15 000yr BP (Junttila, et al., 2010).

The Fennoscandian, Iceland and Greenland ice sheets retreated rapidly from the shelf into the fjords during the Bølling-Allerød interstadials (14 500-13 500yr BP) (Slubowska-Woldengen, et al., 2008; Aagaard-Sørensen, et al., 2010). At the same time, the Svalbard-Barents Sea ice sheet was only present on the Svalbard archipelago, the northwestern Barents Sea basin, Franz Josef Land and Novaya Zemlya (Lambeck, 1996). Slubowska-Woldengen, et al. (2008) found indications of Arctic conditions and proximity of sea ice in the southeastern Barents Sea during this time.

During the Bølling-Allerød interstadials, inflow of saline and chilled Atlantic water on the southwestern and western Svalbard shelf caused the conditions to change from Arctic to Subarctic conditions (Slubowska-Woldengen, et al., 2008). Indications of Arctic conditions, with lower salinity and decreased influence of Atlantic water are observed around Iceland. It is likely an oceanic front, approaching from northwest were in the near proximity of Iceland at the time (Slubowska-Woldengen, et al., 2008). Aagaard-Sørensen, et al. (2010) observed a continuous influence of Atlantic water in Ingøydjupet, off the northern Norwegian coast, in the period 14 200-12 700yr BP.

In the Norwegian Channel and northwards along the southern Norwegian margin, sea surface temperatures (SST) of 7-9°C are recorded (Klitgaard-Kristensen, et al., 2001). This show a significant warming of the SST compared to the previous times, and only slightly lower than temperatures measured today (Slubowska-Woldengen, et al., 2008). Atlantic water did not reach the southern Barents Sea, between Norway and Novaya Zemlya, where sea ice and Arctic conditions dominated during the Bølling-Allerød interstadials (Slubowska-Woldengen, et al., 2008).

About 12 500-11 500yr BP a near glacial period called Younger Dryas occurred. In the northern North Sea, along the Svalbard shelf and in the southeastern Barents Sea the foraminiferal faunal composition indicates freshening and cooling of the shelf bottom waters, indicating a return of Arctic conditions (Slubowska-Woldengen, et al., 2008). High IRD content in the northern North Sea indicates the presence of melting icebergs and/or sea ice (Klitgaard-Kristensen, et al., 2001).

There are indications of subsurface inflow of Atlantic water north of Iceland during the Younger Dryas (Slubowska-Woldengen, et al., 2008). Indications of the proximity of an oceanographic front are observed on the Svalbard shelf, moving north from Iceland since the Bølling-Allerød interstadials (Slubowska-Woldengen, et al., 2008).

2.3.2 The Holocene

The Holocene is the interglacial time-period from about 11 700yr BP to recent.

In the period 11 000-9800yr BP Risebrobakken et al. (2010) suggests a strong stratification of the surface/subsurface and bottom water masses in the southwestern Barents Sea. From 10 900yr BP to 9300yr BP indications of a common origin of the water masses consisting of

Atlantic water are present in Ingøydjupet (Aagaard-Sørensen, et al., 2010). Indications of a warming of the bottom water flowing north, to the southwestern Barents Sea, are recorded at the same time (Risebrobakken, et al., 2010; Groot, et al., 2014). In the period 9800-7500yr BP indications of enhanced winter mixing of the water masses, with strong influence of Atlantic water (Aagaard-Sørensen, et al., 2010), and a strengthened air-sea interaction are observed (Risebrobakken, et al., 2010).

In the late early Holocene (9500-7500yr BP), a strong inflow of warm and saline Atlantic water entered the Nordic, and Barents Seas. As the Atlantic water flowed north, the temperature dropped and indications of a strong influence of chilled and saline Atlantic water along the western and northern Svalbard shelf and northern Barents Sea shelf reaching into St. Anna Trough is present (Slubowska-Woldengen, et al., 2008). Slubowska-Woldengen, et al. (2008) suggests this as indications of strengthening of the West Spitsbergen Current (WSC).

In the southeast Barents Sea indications of enhanced inflow of warm Atlantic water through the NCaC is observed in foraminiferal assemblages (Slubowska-Woldengen, et al., 2008). On the northern Iceland shelf, foraminifera indicate strong influence of Atlantic water (Slubowska-Woldengen, et al., 2008). Klitgaard-Kristensen, et al. (2001) suggests a strong increase of bottom water temperatures in the North Sea during the late early Holocene (9500-7500yr BP). The Arctic Front is suggested to be located close to the southwestern Barents Sea margin (Risebrobakken, et al., 2010) and in the proximity of the northern and western Svalbard shelf respectively during the late early Holocene (Slubowska-Woldengen, et al., 2008) .

During the mid Holocene (7500-2500yr BP) the sea surface temperature (SST) is believed to be above the present day temperatures. However, a cooling trend from the early Holocene maximum SST to the late Holocene (2500-0yr BP) minimum SST is observed (Risebrobakken, et al., 2010). Atlantic water inflow to the southwestern Barents Sea increase during the mid Holocene compared to the early Holocene (Risebrobakken, et al., 2010). Risebrobakken, et al. (2010) suggests that the present day oceanographic patterns in the area were established during the mid Holocene. The water column in the southwestern Barents Sea was well ventilated during the mid Holocene (Risebrobakken, et al., 2010).

In the late mid Holocene (4000-2000yr BP), there are indications of Arctic conditions returning along the Svalbard margin and northern Barents Sea shelf with a reduction in the

influence of Atlantic water compared to the early Holocene (Slubowska-Woldengen, et al., 2008). There is not much change on the Iceland shelf during late Holocene compared to the early Holocene. However, there are some indications of mixing Arctic water masses with Atlantic derived waters on the northern Iceland shelf (Slubowska-Woldengen, et al., 2008).

In the late Holocene (2500-0yr BP) conditions varied with several low salinity episodes, indicating a shift of the transitional zone between Atlantic and Coastal water (Risebrobakken, et al., 2010). During the recent part of the late Holocene there has been one major warming period, the Medieval Warm Period (MWP), lasting from 900AD to 1300AD, followed by a cold period called the little ice age (LIA) lasting from 1300AD to about 1900AD. The MWP is preceded by a cold period called the dark ages cold period (DACP) lasting 400 years, from 400AD to 800AD (e.g. Wilson et al. (2011) and Eiriksson et al. (2000)).

2.4 Benthic foraminifera

Benthic foraminifera are microorganisms living on the seafloor and in the top cm of the sediments. Foraminifera are diverse, with thousands of different species thriving under different temperature, salinity, sedimentary and other conditions. There are two main types of preferred habitats of benthic foraminifera species. They are infaunal species living within the top centimeters of the sediment and epifaunal species living on top of the sediments. This study does not differ between infaunal and epifaunal species.

Foraminifera respond rapidly to changes in their environment, like changes in nutrient supply or temperature and salinity changes. The calcareous foraminifera shell, commonly referred to as the test, are normally frequent and well preserved in sediments, making them ideal for use as biomarkers. Atlantic water has a higher concentration of organic material, and species that prefer a habitat enriched with organic material can be used as an indication of Atlantic water inflow (Knies & Martinez, 2009).

The foraminifera test can be either agglutinated, meaning the organism constructs the test from sediment particles glued together, or calcareous, where the test is constructed of calcium carbonate. In Arctic areas, benthic foraminifera produce smaller test than similar species in temperate areas (Schröder, et al., 1987).

High content of organic carbon is often observed together with a high content of fine particles (e.g. Junttila et al. (2014) and Dijkstra et al. (2013)). As the Atlantic water flows north as a surface current, the organic material begins to sink while being transported northward, eventually reaching the seafloor and become available for benthic foraminifera.

The calcareous tests cannot be found below the carbonate compensation depth (CCD), where all carbonate is completely dissolved in the seawater. The CCD varies in depth throughout the oceans, but it is usually located below 4500m depth on average (Allaby, 2013).

Because benthic foraminifera are sensitive to change they are ideal for use in climatic studies and studies considering changes in the seafloor environment. By comparing a decrease for some species and simultaneously an increase in other species preferring different environmental conditions, it is possible to identify and suggest possible reasons for the change.

2.5 Ecological preferences

For further information on some of the species, see chapter 3.4.1 Taxonomy notes.

2.5.1 *Cribrostomoides* spp. (Cushman, 1910)

Cribrostomoides spp. is an epifaunal, agglutinated species scavenging the sediment surface for nutrients (Linke & Lutze, 1993). *Cribrostomoides* spp. reacts rapidly and utilizes large amounts of organic material from planktonic bloom events (Linke & Lutze, 1993; Struck, 1995). Today *Cribrostomoides* spp. can be found in calm environments with low sedimentation rates (Linke & Lutze, 1993; Khusid & Korsum, 1996).

2.5.2 *Reophax* spp. (Montfort, 1808)

Reophax spp. is an infaunal, agglutinated species. *Reophax* spp. has a long geological history, ranging from the Ordovician to recent (Gutschick, 1986). They are tolerant to poor trophic conditions and are well adapted to low amounts and poor quality organic material (Dessandier, et al., 2015).

Reophax spp. correlates positively with TOC and have a negative correlation with temperature (Hald & Steinsund, 1992).

2.5.3 *Buccella* spp. (Andersen, 1952)

Buccella spp. is suggested to have an association with the submerged inflow of nutrient rich Atlantic water and long ice-free seasons (Jennings, et al., 2011; Slobuwska-Woldengen, et al., 2007).

The association with Atlantic water is not clearly demonstrated in all studies. Polyak and Solheim (1994) found a connection between *B. frigida* and seasonal sea ice cover and moderately to high seasonal productivity. This connection is supported by Hald and Steinsund (1996), which also found that *Buccella* spp. have a fairly wide salinity, temperature and substrate preferences, but generally prefer relatively low temperatures and slightly reduced salinities. They tend to be numerous in areas of high biological activity as they feed on fresh phytodetritus associated with proximity to a seasonal sea ice edge of oceanic front (Slubowska, et al., 2005). *Buccella* spp. can survive in low salinity environments and is commonly found in a sandy substrate (Hald & Steinsund, 1996; Lagoe, et al., 1994).

2.5.4 *Cribroelphidium excavatum* (Terquem, 1875)

Cribroelphidium excavatum, originally identified as *Polystomella excavata* by Terquem (1875) is a species thriving in cold water, often found in glaciomarine sediments (Mackensen, et al., 1985) and in near glacial environments (Hald, et al., 1994). This species is generally known as an Arctic species (Polyak & Solheim, 1994; Austin & Sejrup, 1994). Several subspecies of *C. excavatum* have been proven (Feyling-Hanssen, 1972) and it is worth noting the widespread occurrence of the cold water thriving sub species *C. excavatum* f. *clavata* (Cushman, 1944) found in shallow Arctic water (Hald & Vorren, 1987).

C. excavatum is known to be a tolerant eurytopic species (Conradsen, et al., 1994; Austin & Sejrup, 1994). The appearance of *C. excavatum* has a positive reaction to variation in salinity, temperature and in turbulent waters (Conradsen, et al., 1994; Hald, et al., 1994).

It is a very opportunistic species, capable of surviving in shifting environments with prevailing low salinities and/or temperatures and high turbidity (Hald & Steinsund, 1996). Linke and Lutze (1993) considered *C. excavatum* a highly adaptable species, adapting according to changes in nutrient supply and other environmental factors.

Cribroelphidium incertum, often referred to as *Elphidium incertum*, is considered a good indicator for brackish water and is often mentioned in connection to river proximal settings and brackish environments (Hald & Steinsund, 1996; Polyak, et al., 2002).

2.5.5 *Cassidulina laevigata* (d'Orbigny, 1826)

Living *Cassidulina laevigata* is reported from latitudes ranging from 50°N up to 73°N (Sejrup, et al., 2004). It prefers habitats with incoming water of oceanic (i.e. Atlantic) origin and avoids areas with fine grained sediments (Klitgaard-Kristensen, et al., 2002; Mackensen & Hald, 1988). *C. laevigata* prefers turbulent and well-oxygenated water and avoids areas with low oxygen content (Klitgaard-Kristensen, et al., 2002). Warm and high salinity bottom water of Atlantic origin and a sandy substrate is considered favorable conditions for *C. laevigata* (Mackensen & Hald, 1988). *C. laevigata* is morphologically similar to its northerly relative *C. neoteretis* (Mackensen & Hald, 1988).

2.5.6 *Cassidulina neoteretis* (Seidenkrantz, 1995)

Cassidulina neoteretis were first identified as *Cassidulina teretis* by Tappan (1951). Using a light microscope and images taken by a scanning electron microscope (SEM) the two species were identified separately (Seidenkrantz, 1995). *C. teretis* (Tappan, 1951) is considered extinct in the north Atlantic since about 0.7 million years ago (Seidenkrantz, 1995).

C. neoteretis is associated with fine grained, organic rich sediments often with terrigenous mud (Mackensen & Hald, 1988). *C. neoteretis* have been found to prefer chilled Atlantic intermediate water with relatively low salinity and low turbidity (Mackensen & Hald, 1988; Hald & Steinsund, 1996; Slubowska, et al., 2005). Temperatures above 5°C are believed to restrain the distribution (Hald & Steinsund, 1996). It is often found together with high concentrations of planktic foraminifera, suggesting they pursue phytoplanktic blooms (Slubowska, et al., 2005).

It thrives in cold water conditions and it can be used as an indication of glaciomarine paleoenvironments (Mackensen & Hald, 1988).

2.5.7 *Cassidulina reniforme* (Nørvang, 1945)

Cassidulina reniforme is a shallow infaunal opportunistic species found in glaciomarine environments (Elverhøi & Bomstad, 1980; Mackensen, et al., 1985). It prefers cold water temperatures and a muddy substrate. *C. reniforme* tolerates periods of oxygen depletion

(Mackensen, et al., 1985; Mudie, et al., 1984; Sejrup, et al., 1981; Hald & Vorren, 1987; Polyak, et al., 2002) and is often found together with *C. excavatum* as it is associated with Arctic areas (Hald, et al., 1994; Khusid & Korsum, 1996).

Due to its small size, it is susceptible to downslope redeposition in sandy muds (Mudie, et al., 1984). *C. reniforme* is thriving in areas with rapid sedimentation of terrigenous material (>1cm/ka) (Sejrup, et al., 1981; Khusid & Korsum, 1996).

2.5.8 *Islandiella norcrossi* (Cushman, 1933)

Islandiella norcrossi is associated with cold Arctic water, distal glaciomarine sediments enriched in IRD and marine mud (Korsun & Hald, 1998; Eiriksson, et al., 2011). This Arctic species is associated with a seasonal sea ice cover, often proximal to a sea ice edge, and with relatively high and stable bottom water salinities (Polyak & Solheim, 1994; Korsun & Hald, 1998).

2.5.9 *Eilohedra nipponica* (Kuwano, 1962)

Eilohedra nipponica is an epifaunal species, living on top of the sediments (Wollenburg & Mackensen, 1998). In literature, the species is commonly referred to as *Epistominella nipponica*.

It is a small and round, generally <150µm, seasonally opportunistic species (Usami, et al., 2013). Due to their small and round size, they are easily transported by high bottom current speeds and are considered a fragile species (Murray, et al., 1982; Hald & Steinsund, 1992; Saher, et al., 2012). *E. nipponica* is considered a warm species, preferring saline waters with temperatures >4°C, common found in soft mud enriched with organic material (Hald & Steinsund, 1996; Saher, et al., 2012).

2.5.10 *Lobatula lobatula* (Walker & Jacob, 1798)

Lobatula lobatula, often mentioned by its synonym *Cibicides lobatulus*, is considered an epifaunal species, found in coarse-grained sediments with an organic carbon content of 1-3mg/g dry sediment (Klitgaard-Kristensen, et al., 2002). Being a suspension-filter feeder it prefers coarse grained, high-energy environments where it can cling to gravel, crustaceous shells and similar to filter the water (Hald & Steinsund, 1996; Conradsen, et al., 1994; Mackensen, et al., 1985).

The occurrence of *L. lobatula* is restricted by low salinities, but not by temperature (Hald & Steinsund, 1996). *L. lobatula* is primarily useful for indicating strong bottom currents.

2.5.11 *Melonis barleeanus* (Williamson, 1858)

Melonis barleeanus are associated with fine-grained sediments, typically rich in organic material and nutrients (Polyak & Solheim, 1994; Jennings, et al., 2011; Hald & Steinsund, 1996). Its occurrence is tied to Atlantic derived waters (Mudie, et al., 1984). It prefers partly degraded organic matter, commonly originating from redeposition from shallow areas, as a source to nutrients (Caralp, 1989) .

Hald and Steinsund (1996) found that temperature does not seem to significantly affect the distribution of *M. barleeanus*, however low salinities were found to be a restrictive parameter.

Occurrence of the infaunal species, *M. barleeanus*, can indicate increased marine productivity and burial of nutrients (Jennings, et al., 2011).

2.5.12 *Nonionella* spp. (Dawson, 1860)

Nonionella spp. are grouped together to avoid taxonomic uncertainties, see section 3.4.1. Taxonomy notes.

Nonionella labradorica is a deep infaunal species, associated with fine-grained sediments enriched in organic material (Conradsen, et al., 1994; Corliss, 1991). Conradsen et al. (1994) found that *N. labradorica* prefers salinities between 30‰ and 35‰. *N. labradorica* feeds on fresh phytodetritus and its presence may reflect high primary productivity as a result of the retreating summer sea ice margin or Arctic Front (Jennings, et al., 2011). *N. labradorica* and *N. auricula* both prefer colder bottom water with temperatures less than 2°C (Wilson, et al., 2011).

N. turgida, originally named *Rotalina turgida* by Williamson (1858), is associated with long ice-free seasons and submerged inflow of nutrient rich Atlantic water (Jennings, et al., 2011; Polyak & Mikhailov, 1996). It is a deep infaunal species, living 4cm and deeper in the sediment (Corliss, 1991).

3 Material and methods

This section cover materials and methods used to obtain data and information from the cores. All the cores were sampled at 1cm intervals except the two lowest samples in core 993 that were sampled at 1.5cm intervals (appendix 2). In total 100 samples were investigated. Only the bottom parts of the cores (Table 2) are used for the purpose of this study. The top halves of the cores are studied by Dijkstra et al. (2016).

For practical and simplifying reasons, the cores are referred to as the number in the core name in the text (Table 2), e.g. core HH12-903-MC will be referred to as core 903.

Core name	**Date**	**Location**	**Latitude (N) Longitude (E)**	**Water depth (m)**	**Sample interval (cm)**
HH12-903-MC	14.07.2012	Sentralbanken south	74°04.961757N 034°30.091517E	323	20-45
HH12-902-MC	13.07.2012	Sentralbanken south	73°57.844N 033°48.926E	333	20-44
HH12-897-MC	12.07.2012	Sentralbanken south	73º18.983N 030º15.714E	361	20-40
HH12-893-MC	11.07.2012	Bjørnøyrenna south	72º51.441129N 24º18.658116E	435	20-41
IG15-993-MC	20.06.2015	Bjørnøyrenna West	7220.144125N 01809.412879E	380	20-31

Table 2: Core information gathered from the cruise reports.

3.1 Sampling

The cores were retrieved using a multicorer on cruises with RV Helmer Hanssen, operated by UiT, in 2012 and 2015 (Table 2).

The multicorer retrieves several cores in one coring, which is one of the advantages with the multicorer. Because several cores are retrieved at the same time, the chance of at least one successful core increase. The core length possible to achieve with a multicorer is limited, usually to less than one meter per core.

3.2 Freeze drying

The cores were sampled in plastic bags, at one cm intervals, with the exception of the two lowest intervals in core 993, which were sampled at 1.5cm intervals (appendix 2). All the samples were weighed to gain the wet weight to be used in later calculations. The samples

were placed in a freezer until completely frozen. The frozen samples were then placed in a freeze-dryer for about 24 hours.

The freeze-dried samples were weighed using a certified two decimal scale, Sartorius AG ED2202S-CW, in order to calculate the water content in the samples. The freeze dryer used is a CHRIST ALPHA 1-4 LSC plus freeze dryer.

Freeze-drying works by vaporizing the ice in the frozen sample without turning it to liquid water. Freeze-drying is preferable to oven drying as it removes the water without altering the structure of the sediments. Foraminifera tests are better preserved using freeze-drying because contraction of the sediments during drying is avoided. In addition, sediments containing clay are easier to handle after freeze-drying as they become and stay friable.

3.3 Sieving

Before sieving the samples, each sample was subsampled three times. The subsamples were 2-3g, and were used for the grain size analysis, TOC analysis and one reference sample in case something should go wrong when handling the other samples, and for future references.

Sieving is a method used for separating the different size fractions. The process can be done by dry sieving or wet sieving the samples. Wet sieving is used for the purpose of this study.

The remaining material, after the subsampling, was sieved using sieves with mesh sizes of 1mm, 100µm and 63µm. any material smaller than 63µm were not retained. When the samples appeared sufficiently clean, they were transferred from the sieves to a labelled special filter paper for excess water to run off.

The sieves were cleaned between the samples using an ultrasound bath followed by high water pressure to remove any possible particles stuck in the mesh.

The sieved samples were dried overnight in a dry-cabinet at 40°C, before being transferred to glass vials. The glass vials were weighed using the same two decimal scale used in the freeze-drying process, before and after the sample were transferred to the vials. This was done to retrieve the dry weight of the samples of the different fractions.

Using this preparation method can introduce error margins. One such error margin can be using too high water pressure, which can destroy the tests. Another possible error margin is not properly cleaned sieves or small holes in the sieves.

3.4 Foraminiferal analysis

To get a representative species assemblage of benthic foraminifera the mesh size of 100µm was used for sieving (Knudsen & Ausin, 1996). The >100µm size fraction is the most used size fraction when it comes to identifying foraminifera in Arctic regions, hence the 100µm to 1mm fraction is used for identifying foraminifera to allow a direct comparison with previous studies in the area.

A minimum of 300 specimens per sample were picked and identified in order to determine the relative abundance of the species in the foraminiferal assemblage. The relative abundances are based on the calcareous taxa only, unless otherwise stated in the text. At least 300 counted specimens are considered to provide sufficient accuracy for scientific quantitative examinations (Patterson & Fishbein, 1989). For samples with fewer than 300 specimens in total, the whole sample volume was picked. A sample splitter was used to measure the amount of the sample used for picking and identifying foraminifera in order to calculate the total amount of foraminifera in the sample. The splitter splits the sample in a credible 50/50 split. The calculated total amount of foraminifera is used to calculate the flux. The foraminiferal absolute abundance (total number foraminifera per gram dry sediment) for both calcareous and agglutinated species was calculated. The dry bulk densities (g/cm3) were calculated from the weight measurements.

*Foraminifera flux (number/cm^2*ka) = absolute abundance (#/g)*dry bulk density (g/cm^3)*sedimentation rate (cm/ka)*

The flux gives an indication of the presence of a given species, not relative to the other species, which differs from the abundance, that consider species relative to one another.

The picking itself was done by using a needle with a hair from a paintbrush attached. The hair was dipped in water to improve the surface tension in order to make the foraminifera test stick to the hair. The known sample split was evenly distributed on a picking tray before the foraminifera tests were identified and placed in a microslide for future storage. The microscope used for identifying foraminifera was a binocular microscope, LEICA MZ 12.5. The entire picking tray was counted for all the samples. The sample splitter was used to reduce the amount of material on the tray.

Both calcareous and agglutinated species were picked and identified according to the World Register of Marine Species (WoRMS) and foramnifera.eu webpages, which are based on identifications by Ellis & Messina (1940-1978) and Loeblich & Tappan (1987). The foraminifera were identified down to species level, with the exception of species belonging to *Reophax, Buccella* and *Cribrostomoides*. Those species were identified to genus level and grouped together as *Reophax* spp., *Buccella* spp. and *Cribrostomoides* spp. respectively. Many of the agglutinated species tests were broken, in which case three identifiable pieces were considered equal to one theorized foraminifera test. One of the pieces should preferable show the aperture.

Error margins can occur using the sample splitter, as there is a slight chance the sample might not be split in exactly 50/50. Also small amounts of the sample can attach to the splitter itself due to static electricity. There is also a small chance of overlooking some foraminifera while picking.

3.4.1 Taxonomy notes

The *Reophax* spp. is identified to genus level to avoid mixing of the species given that most of the tests were broken.

Buccella spp. is identified to genus level because of their similar ecological preferences and to eliminate the potential error in the identification and mixing of the species (e.g. Slubowska et al. (2005)). It is assumed a predominance of *Buccella frigida* Cushman (1952).

C. excavatum is grouped together with *C. incertum* to avoid taxonomic uncertainties. The subspecies have been overlooked and simply classified as *C. excavatum* for the simplicity of this thesis.

The *I. norcrossi* group includes *I. norcrossi* and *I. helenae*. They are grouped together to avoid taxonomical uncertainties due to their transitional morphology making them difficult to distinguish. It is common to count these two species together as one species (e.g. Korsun & Hald, 1998).

It should be noted that *E. nipponica* is almost morphologically identical to the temperature tolerant species *Alabaminella weddellensis*, usually found in deeper waters (Saher, et al., 2012; Jennings, et al., 2011).

Nonionella spp. consist of *N. labradorica* grouped together with *N. turgida* and *N. auricula* to avoid taxonomic uncertainties and allow better comparison with previous studies where combining these species is common (e.g. Saher et al. (2009), Hald & Steinsund (1996) and Wilson et al. (2011)). *N. labradorica* is the most abundant species of the three, thus having the most impact on the observed signal.

3.5 Dating

Foraminifera tests from the top and bottom of all the core sections were sent to Poznan Radiocarbon Laboratory, located in Poznan, Poland, for Accelerator Mass Spectrometry (AMS) ^{14}C Dating. Only the calcareous tests were sent for dating.

The minimum amount of calcareous material possible to date, according to the Poznan laboratory, is 2mg. The samples consisted of various calcareous species collected from a range interval (Table 4).

The principle behind AMS ^{14}C dating is measuring ^{14}C atoms relative to ^{12}C and ^{13}C. ^{14}C is the only unstable, radioactive, isotope of the carbon atom, with a half-life of 5700 ± 30yr (Goddard, et al., 2016). It is possible to date 50 000-60 000yr, in some cases with sufficient material and the best available equipment it is theoretically possible to date as far as 75 000yr using AMS ^{14}C dating.

AMS ^{14}C works by accelerating electrically charged particles to high velocities and exposing them to a strong magnetic field. The electrically charged particles are deflected as they pass the magnetic field. The heavy particles (^{14}C) deflect less than light particles (^{12}C and ^{13}C), enabling the spectrometers to detect the number of atoms based on the angle of deflection (Purser & Litherland, 1990).

CALIB 7.1.0 was used to calibrate the ^{14}C ages into years BP (before present, 1950AD). Using the MARINE13 radiocarbon calibration curve the calibrations are limited to 50 000yr. CALIB 7.1.0 uses a modeled ocean with a global reservoir correction age of about 400yr and to accommodate the local effects (Delta R) in the study area a delta R value of 67±34yr was used (Mangerud & Gulliksen, 1975). This delta R age was retrieved from CALIBs own database for local reservoir correction ages.

When calibrating radiocarbon datings 1950 AD is considered the start of the present. This is because of all the excess ^{14}C that entered the atmosphere originating from nuclear explosions and accidents in the years after 1950 AD.

Some complications with the calibration are the fact that the atmospheric production of ^{14}C is inconsistent through time. This influence the length of ^{14}C years, making them differ from calendar years. As water masses of different ^{14}C ages are circulating in the oceans, a correction is needed for a given area. This correction is called the reservoir effect and is defined as the difference between ^{14}C ages in the oceans and atmosphere at any given time (Stuvier, et al., 1986). The ^{14}C relationship between the ocean and the atmosphere interface is relatively constant, while the amount of ^{14}C available can vary. Marine organisms incorporate ^{14}C from the surrounding water and upwelling of old deep water cause a dilution in the area of upwelling causing organisms to reflect a younger age (Mangerud, et al., 2006; Stuvier, et al., 1986). Due to these processes and the possibility of the sediments being reworked, the calibrated ages should always be considered as minimum ages.

3.6 Organic Carbon

Before measuring the total organic carbon (TOC) the samples had to be prepared.

3.6.1 Sample treatment

The samples were crushed to a fine powder using a Retsch GmbH - Mortar Grinder RM-100. About 0.45g of each sample were weighed and placed in crucibles for chemical treatment to remove any inorganic carbon.

The samples were covered with 10% hydrochloric acid (HCl), to remove the inorganic carbon, and placed in a fume hood where they were left over night for the acid to work. The samples were then washed eight times using distilled water to remove any remaining acid, which fumes can disturb and possibly destroy the sensors in the LECO analyzer.

3.6.2 LECO Analysis

The total organic carbon (TOC) was measured using a LECO CS 744 combustion analyzer, at the geology laboratory at the University of Tromsø. The LECO CS 744 incinerates the sample and analyzes the fumes. Both carbon and sulfide content are measured, but only the carbon results are of interest to this study.

A minor amount of iron and LECOCEL accelerator were added to the crucibles to act as accelerators during the incineration. The samples were, one after one, placed in the furnace and incinerated to obtain the TOC concentrations. The analysis was preformed two times. One time using chemically treated samples to obtain the TOC values, and one time, without any chemical treatment, to obtain total carbon (TC) values. 0.45g of sample material was used for the TOC analysis and 0.23g for the TC analysis.

3.7 Particle size analysis

The particle size analysis (PSA) was executed in the geology laboratory at UiT using a Beckman Coulter LS 13320 Particle Size Analyzer. This particle size analyzer use laser diffraction to count individual grains between 0.04µm and 2mm.

3.7.1 Sample treatment

About 2g of all the samples were weighed and placed in individually marked plastic tubes for chemical treatment to remove calcium carbonate ($CaCO_3$) and organic material. The particle size analyzer does not differ between the grains, calcium carbonate particles and the organic material particles. By removing calcium carbonate and organic material an accurate measurement of the grainsizes present in the samples can be obtained.

All samples were treated chemically using HCl and hydrogen peroxide (H_2O_2) to remove calcium carbonate and organic material respectively.

The samples were covered with 20% HCl and put under a fume hood for 24 hours to remove calcium carbonate from the samples. After 24 hours, when the calcium carbonate was removed, the samples were centrifuged for four minutes at 4000rpm, and all excess acid were properly disposed of. The tubes were filled with distilled water and centrifuged again to wash the samples. All samples were washed twice to make sure any leftover HCl were removed.

After removing the calcium carbonate, the samples were covered with 20% hydrogen peroxide to remove organic material. The tubes containing the samples covered with hydrogen peroxide were covered with aluminum foil and placed in water at 80°C to speed the chemical reaction. The samples were left in the water for two hours, until the reactions had stopped. Figure 6 shows the tubes containing the samples, reacting with hydrogen peroxide. To avoid cracking of the tubes during the centrifuging and washing process, the tubes were cooled to approximate room temperature. The washing process is the same as for the HCl

treatment, centrifuging for four minutes at 4000rpm and washing with distilled water two times.

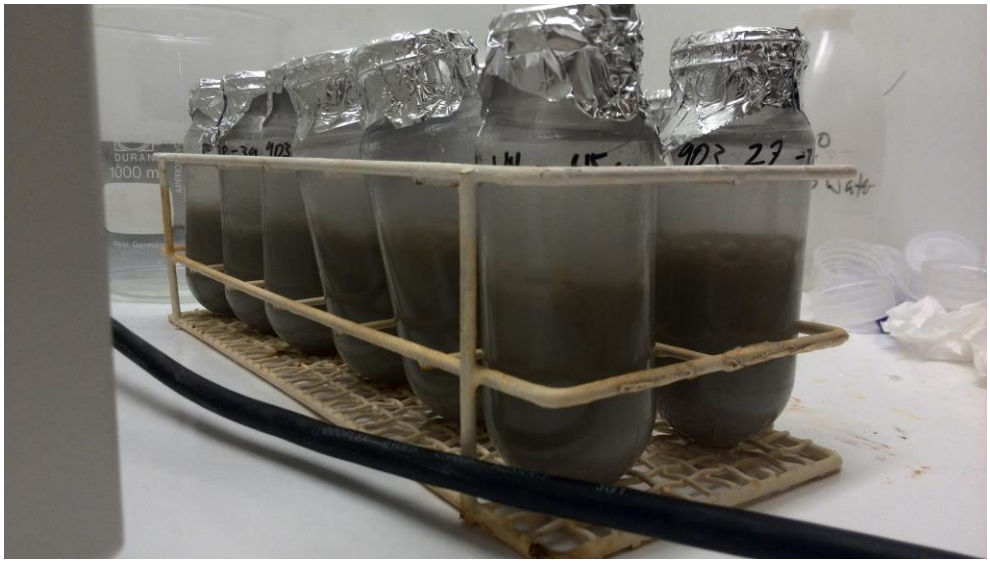

Figure 6: The tubes with sample material reacting with hydrogen peroxide, removing organic material.

After the acid treatments, the samples were transferred to plastic cups and stored in a freezer to prepare the samples for freeze-drying. The samples were freeze-dried in order to dissolve the samples readily in water. 0.5mg of the sample material were transferred to a new plastic cup and 20cl water was added. The plastic cups were placed in an Edmund Bühler GmbH SM-30 universal shaker over night to keep the material in suspension and avoid flocculation of the particles. Before analyzing the samples, two drops of a calgon solution were added to remove the surface tension of clay particles.

3.7.2 Sample analysis

The chemically treated samples were put in an ultrasound bath for five minutes before being poured, one at the time, through a 2mm sieve, in to the particle size analyzer. Each sample was analyzed three times to get a representative measurement of the entire sample. The average result of the three measurements was used for calculating statistics on the grainsize.

All grainsizes are referred to as they are classified after the Udden-Wentworth scale classification scheme (Figure 7). The grainsize fraction smaller than 63µm may be referred to as mud.

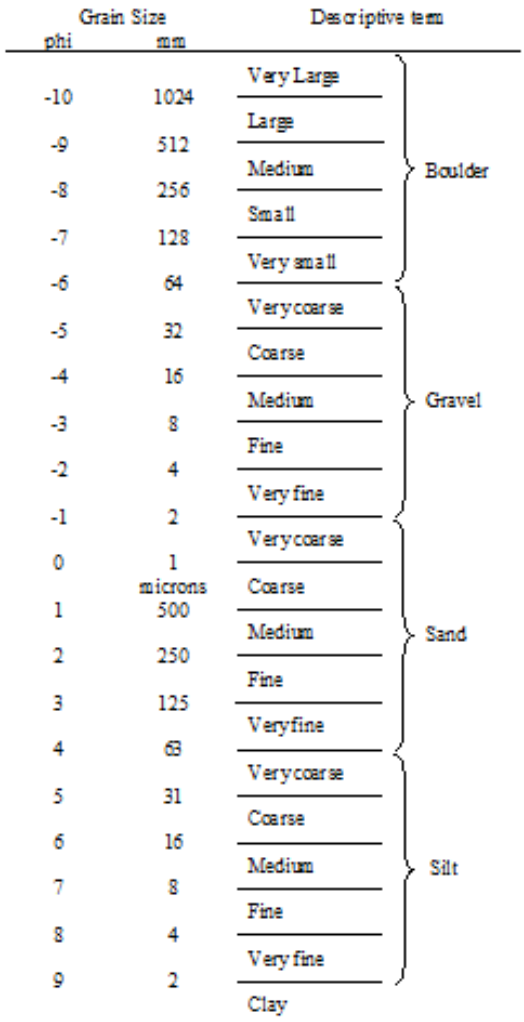

Figure 7: The Udden-Wentworth size scale. Figure retrieved from GRADISTAT 8.0.

Possible error margins can be flocculated particles and leftovers of organic material or calcium carbonate, which can influence the measured result.

3.8 Data processing

The results from the PSA were used to retrieve statistical data using a macro-activated excel spreadsheet, developed by Dr. Simon J. Blott, called GRADISTAT 8.0 (Blott, 2010). Statistics regarding mean grainsize, sorting, skewness, kurtosis, percentage of each grainsize between 0.04µm and 2mm and percentage of the descriptive term, after the Udden-Wentworth classification scheme (Figure 7), are obtained.

For the purpose of this study, the geometric methods of moments statistics were used. The statistical formulas used to calculate the statistics are given in Table 3.

Mean	Standard Deviation	Skewness	Kurtosis
$\bar{x}_g = \exp \frac{\Sigma f \ln m_m}{100}$	$\sigma_g = \exp \sqrt{\frac{\Sigma f (\ln m_m - \ln \bar{x}_g)^2}{100}}$	$Sk_g = \frac{\Sigma f (\ln m_m - \ln \bar{x}_g)^3}{100 \ln \sigma_g^3}$	$K_g = \frac{\Sigma f (\ln m_m - \ln \bar{x}_g)^4}{100 \ln \sigma_g^4}$

Table 3: Statistical formulas used by GRADISTAT 8.0 to calculate the geometric methods of moments. f=frequency in percent, m=mid-point of interval in metric or phi intervals. Table from GRADISTAT 8.0

All graphs presented in this thesis are produced using the Grapher 9 software.

3.8.1 Sortable silt

GRADISTAT v8.0 was also used to get statistics on sortable silt ($\overline{SS}$). To obtain information on the sortable silt, the silt fraction from the analysis were treated separately statistically. The silt fraction is the grainsizes from 2µm to 63µm (Figure 7).

The smallest grainsizes like clay and fine silt particles are known to flocculate, creating aggregates. These aggregated may not behave in an interpretable way, and sortable silt is therefore defined as the silt fraction between 10µm and 63µm (Hass, 2002). Any grains larger than 63µm are considered too heavy for the deep-sea currents to transport in suspension over long distances, and can be assumed ice rafted (Hass, 2002).

The mean sortable silt grain size ($\overline{SS}$) exclusively depends on bottom current strength, and the difference in sediment input can be ignored (Hass, 2002). Large $\overline{SS}$ sizes show stronger bottom currents than small $\overline{SS}$ sizes.

In cases with a high ice rafted debris (IRD) content, the $\overline{SS}$ needs to be corrected for ice rafted silt influence. This is done by correlating the $\overline{SS}$ and sand (%). If $\overline{SS}$ and sand (%) is correlatable it suggest a similar mode of transportation (Hass, 2002). Creating a regression function, showing $\overline{SS}$ primary influenced by ice rafting, from the correlation curve allows the potential $\overline{SS}$ ($\overline{SS}_{pot}$) to be calculated. $\overline{SS}_{pot}$ describes how the $\overline{SS}$ would appear if there were no fluctuations in the current strength. The difference between $\overline{SS}$ and $\overline{SS}_{pot}$, in the coarser or finer direction, give an indication if the current were stronger or weaker than the calculated values respectively. The difference is called $\Delta\overline{SS}$ and shows the relative current speed fluctuations, corrected for IRD influence.

$\Delta\overline{SS} = \overline{SS} - \overline{SS}_{pot}$

$\Delta\overline{SS}$ is the $\overline{SS}$ component modified by current speed, $\overline{\mathrm{SS}}_{\mathrm{pot}}$ is the $\overline{SS}$ of sediment primarily from ice rafting and $\overline{SS}$ is the measured sortable silt mean (Hass, 2002).

4 Results

The various results obtained during processing of all five cores are presented in this section.

4.1 Radiocarbon dating

Ten samples were radiocarbon dated to obtain the age of the bottom and top part of the core sections. The dating results and the calibrated ages, both 1σ and 2σ results, are presented in Table 4. The calibrated median probability age are assumed to be the age of the sample interval closest to the core, meaning where several intervals were used for dating, the interval closest to the rest of the core is assumed to be the median probability age. The ages are extrapolated from the median probability age to get an age for the sample intervals used in the dating.

Figure 8 shows the age of the cores, in calibrated years before present, and the average sedimentation rate in cm per thousand year (cm/ka) relative to the core sites southwest-northeast position. The sedimentation rates are calculated from the calibrated ages of the cores and are assumed constant throughout the cores.

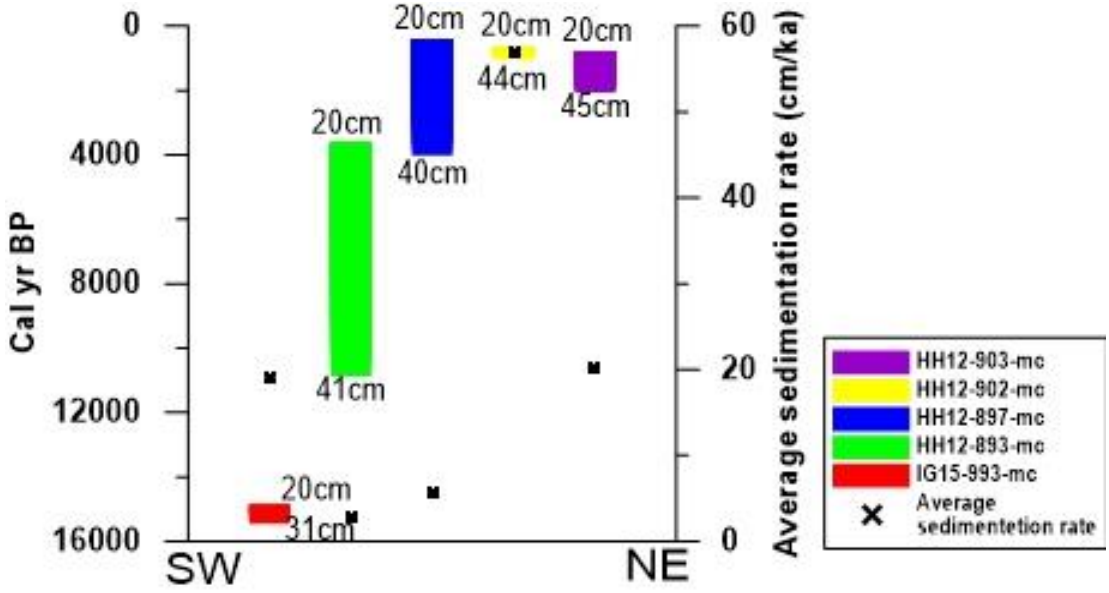

Figure 8: Core age, in cal yr BP, and average sedimentation rate (cm/ka) plotted against the southwest-northeast position of the cores. The top and bottom depth of the cores are given in the figure.

Core	Dated sample interval (cm)	ΔR (year)	Uncalibrated ^{14}C age	Cal age 1σ	Cal age 2σ	Cal age median probability	Extrapolated age
HH12-903-MC	19-20	67 ± 34	1290 ± 30	702 - 816	674 - 881	766	766
	44-45	67 ± 34	2490 ± 35	1988 - 2124	1916 - 2215	2061	2061
HH12-902-MC	20-22	67 ± 34	1135 ± 30	597 - 675	541 - 706	634	615
	41-44	67 ± 34	1520 ± 30	942 - 1048	907 - 1123	1001	1038
HH12-897-MC	20-24	67 ± 34	1495 ± 35	922 - 1030	879 - 1113	978	406
	35-40	67 ± 34	3470 ± 80	3157 - 3372	3021 - 3472	3264	4026
HH12-893-MC	20-24	67 ± 34	4600 ± 40	4675 - 4817	4567 - 4845	4731	3646
	39-41	67 ± 34	9700 ± 120	10 349 - 10 670	10 205 - 10 835	10 513	10 875
IG15-993-MC	20-21	67 ± 34	13 070 ± 120	14 652 - 15 189	14 263 - 15 289	14 877	14 877
	29.5-31	67 ± 34	13 400 ± 70	15 300 - 15 588	15 200 - 15 731	15 453	15 453

Table 4: Results from the AMS ^{14}C dating. Cal age = Calibrated age in years before present (yr BP). The 1σ results show the interval in which the true age is 68.3% likely to lie. The 2σ results show the interval in which the true age is 95.4% likely to lie. The extrapolated ages are based on the median probability age.

4.2 TOC

In general, the highest TOC values are found in core 903, with no values lower than 1.7%, closely followed by core 902, which have the lowest value of 1.4%. Both core 902 and 903 show a similar curve where the values increase with ~0.2% from 39cm to 37cm. The TOC value shows a relatively steady increase from 37cm to the top of both cores (Figure 12).

Core 897 shows a TOC value of around 0.87% varying between a low value 0.83% and high value 0.89 at 28.5cm and 34.5cm respectively. The lowest values appear in the top section of the core and the highest values are located in the lower half of core 897 (Figure 12).

The TOC values in core 893 shows a relative steady decrease towards the top of the core being ~1% in the bottom ending on ~0.9% at the top (Figure 12).

The most southern core, core 993, has a relative stable TOC value of ~0.7% from the bottom to of the core to 25cm, where the TOC value begins to decrease, ending on 0.4% at 23.5cm. The TOC value remains around that value to 21.5cm where it increases to 0.8% at the top of the core (Figure 12).

4.3 Grain size and sortable silt

This section provides a description of the relative grain size distribution and the sortable silt mean grain size. The cores are described starting at the bottom, moving towards the top of the cores.

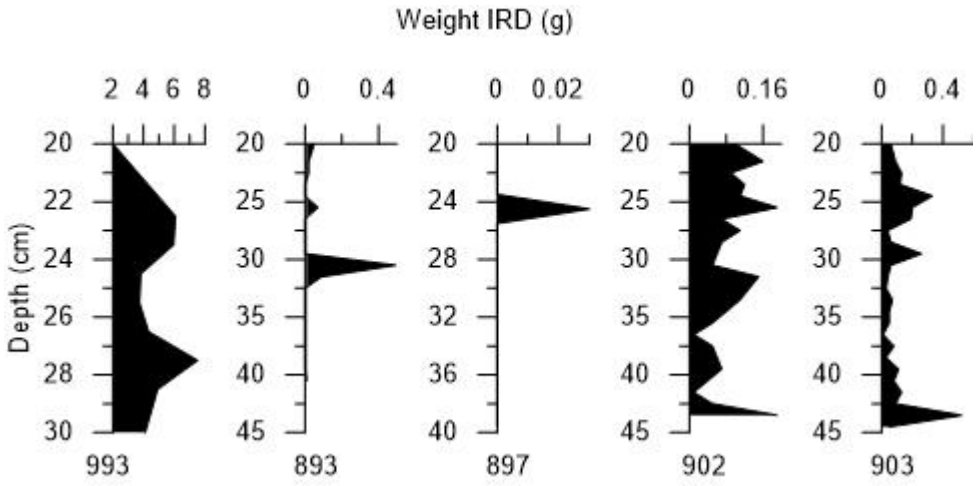

Figure 9: Amount of material >1mm found when sieving. For cores 902 and 903 it mostly consists of organic material.

4.3.1 HH12-903-mc

The percentage of sand in core 903 fluctuates around 7% with two peaks, both over 10%, at 40-41cm and 24-25cm (Figure 12).

The silt content is fluctuating around 75% with the highest values at the top and middle of core 903, just above 78% (Figure 12). Whenever the silt content show a decrease, the clay content show an opposing trend with increasing values.

Clay is fluctuating around 18% with the highest values concentrated between the bottom of the core to 41cm and 25-33cm (Figure 12).

Sortable silt generally fluctuates around 26.3µm throughout the core. A peak at 40-41cm core depth has a sortable silt size of 28.9µm (Figure 12). The highest sortable silt size in core 903 is 29.4µm and found as a peak at 34-35cm. A period of lower sortable silt size is observed between 25cm and 32cm.

The amount of material larger than 1mm (Figure 9) found when sieving was mostly organic material.

4.3.2 HH12-902-mc

The sand content in core 902 starts, from the bottom to the top, with a peak at 42-43cm with a value of 13.7%. The sand content drops to 9.7%, at 39cm, before a relatively steady increase towards the core top. The increase stops at 25cm with a sand content of 13.4% before a drop to 11.4% at the top of the core (Figure 12).

The silt content fluctuates between 66% and 72% from the bottom to 35cm where a general decrease in silt, from about 71.5% to about 68.5%, is observed towards the top of the core (Figure 12).

The clay content shows an increase from the bottom to 42cm where the clay content begins to fluctuate around fluctuate around 21% before the clay content drop to 18% at 35cm and continue to fluctuate around that value to the top of the core (Figure 12).

The sortable silt fluctuates between 25.5µm and 27µm throughout the core with high peaks at the bottom, 32cm and 24cm and low peaks at 40cm and 37cm (Figure 12).

The amount of material larger than 1mm (Figure 9) found when sieving was mostly organic material.

4.3.3 HH12-897-mc

The content of sand in core 897 is fluctuating between 6% and 16% with three distinct high peaks of about 16% at 37-38cm, 33-34cm and 24-25cm. A period of low sand content is observed in the middle of the core, corresponding to a period with high silt content (Figure 12).

A general increase in the silt content from the bottom to 32cm, 74% to 78.5% respectively is observed, with a high peak of 80% at 36cm. From 32cm the silt content shows a general decrease up core to about 73% at 22-23cm depth. The silt content shows an increase to 78.5% at the top of core 897 (Figure 12).

The general pattern of the clay content is a decrease towards the top. The clay content shows low values around 10% from the bottom up to about 34cm where the clay content reaches just above 18%. From 34cm the clay content shows a decrease towards the top, ending on just over 10% (Figure 12).

The sortable silt fluctuates between 26µm and 31µm throughout the core with a decreasing trend from about 33cm to the top of the core. There is a high peak worth taking note of at 37cm with a sortable silt size of 31µm (Figure 12).

A minor amount (0.03g) of IRD was found at 24.5cm core depth (Figure 9).

4.3.4 HH12-893-mc

The sand content fluctuates around 7% throughout the core, with the exception of a high peak of 27.7% at 37-38cm (Figure 12).

The silt content shows a general increase from 70% at the bottom to just below 76% at the top. A low peak is present at 37-38cm at 61.3%, the same depth a high peak in observed in the sand content (Figure 12).

The lowest clay content, in general, is located in the lower half of the core, with the exception of a high peak of 25% at the bottom. In general, the highest clay content is observed in the top half of the core (Figure 12).

The general trend of the sortable silt in core 893 is a decrease in sortable silt size from the bottom to the top. At the bottom there is a low peak of 22.5µm, immediately increasing to 30µm at 39cm before the general decrease begins (Figure 12).

A minor amount (0.5g) of IRD was found at 30.5cm core depth (Figure 9).

4.3.5 IG15-993-mc

The sand content in core 993 shows a general increase from the bottom to the top of the core, starting at 9%, ending on about 20% (Figure 12). In addition, a significant amount of IRD (2-8g) were found during sieving (Figure 9).

The general pattern for the silt content shows a steady decrease from the bottom to 26cm. From 26cm, the silt content fluctuates between 60% and 66% to the top of the core (Figure 12).

The content of clay is highest at the bottom and middle part of the core, fluctuating around 20%. From 24cm to 22cm, the clay content drop to 15% before increasing to 18% at the top of the core (Figure 12).

Because of the Late Glacial age, the amount of IRD (Figure 9), and the poor correlation between sand and sortable silt, $\Delta\overline{SS}$ is calculated for core 993. By plotting the measured sand content (%) against the measured $\overline{SS}$ mean grain size (µm) the average relationship between the two fractions is found by a linear regression line (Figure 10). A linear regression line was chosen as it appear to be the best fit for the data set (Figure 10). The r^2 value of 0.26 indicates a poor correlation between the sand and $\overline{SS}$ mean grain size (µm). An increase in sand content relative to silt content will give a lower $\Delta\overline{SS}$ signal compared to the measured $\overline{SS}$ and vice versa (Hass (2002) and references therein).

The sand value is substituted for X in the linear regression equation Y (Figure 10) to find $\overline{SS}_{pot}$, which is needed to calculate $\Delta\overline{SS}$.

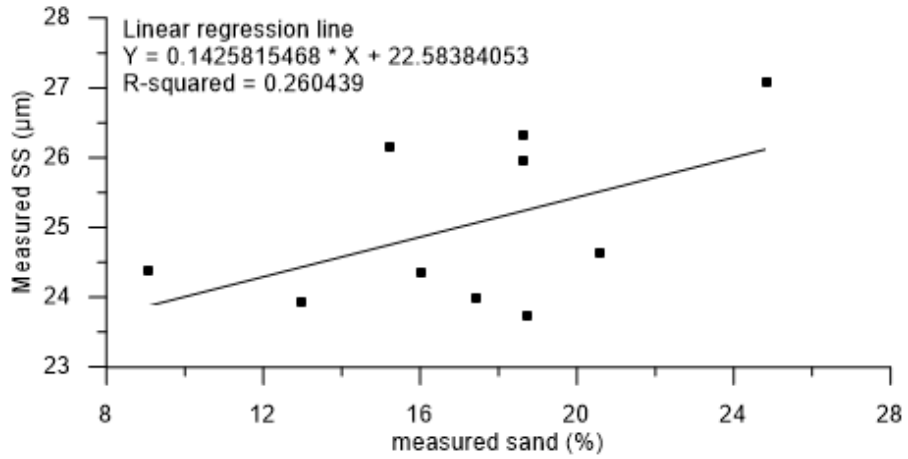

Figure 10: Measured sand content (%) plotted against the measured sortable silt (µm). A linear regression line based on the data points is shown in the figure, from core 993.

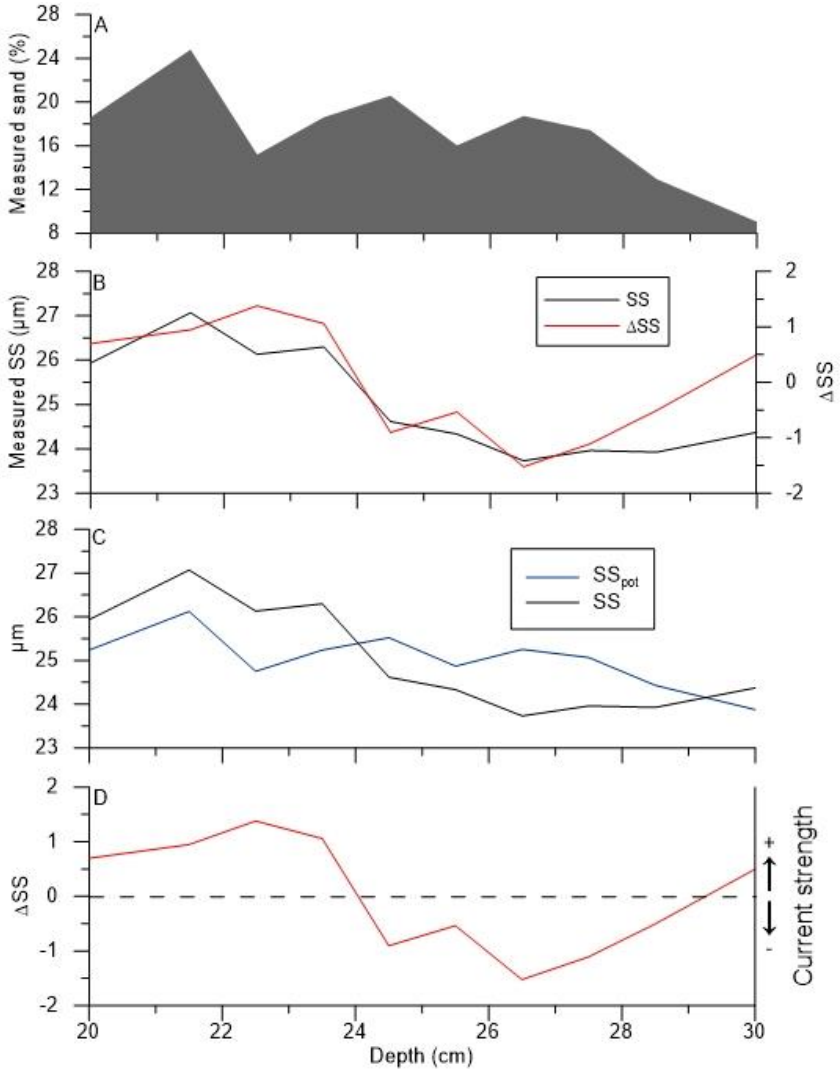

Figure 11: A and B shows the connection between sand (%), $\Delta\overline{SS}$ and the measured $\overline{SS}$ in core 993. C shows the measured $\overline{SS}$ and the $\overline{SS}$pot. D shows the current sorted fraction of the sortable silt mean grain size in core 993

Calculating $\Delta\overline{SS}$ is done by using the equation $\Delta\overline{SS} = \overline{SS} - \overline{SS}_{pot}$. Positive and negative $\Delta\overline{SS}$ values indicate an increase or decrease, respectively, in bottom current strength (Figure 11D). For core 993, $\Delta\overline{SS}$ indicate stronger currents in the top half (Figure 11D).

As seen in Figure 11B, the measured sortable silt correlates well with the calculated $\Delta\overline{SS}$. The observed result shows a decrease from the bottom to about 26cm core depth. In general, the lowest sortable silt size is observed in the lower half and the highest in the top half of the core.

There is a poor correlation between the measured $\overline{SS}$ and $\overline{SS}_{pot}$ (Figure 11C), where they show opposite trends from the bottom to 23cm where they begin to show a similar trend to the top of core 993.

Figure 12: continues on next page

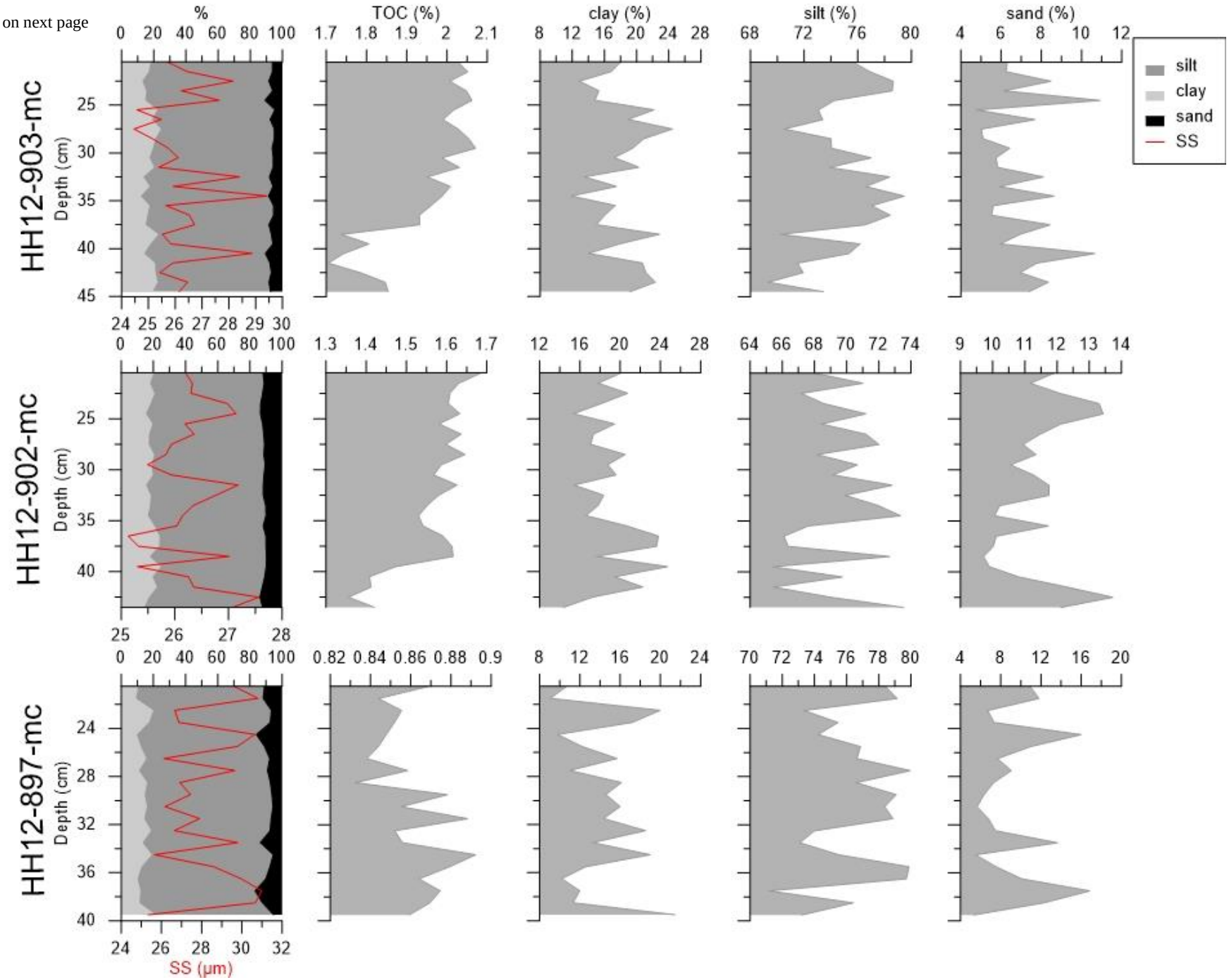

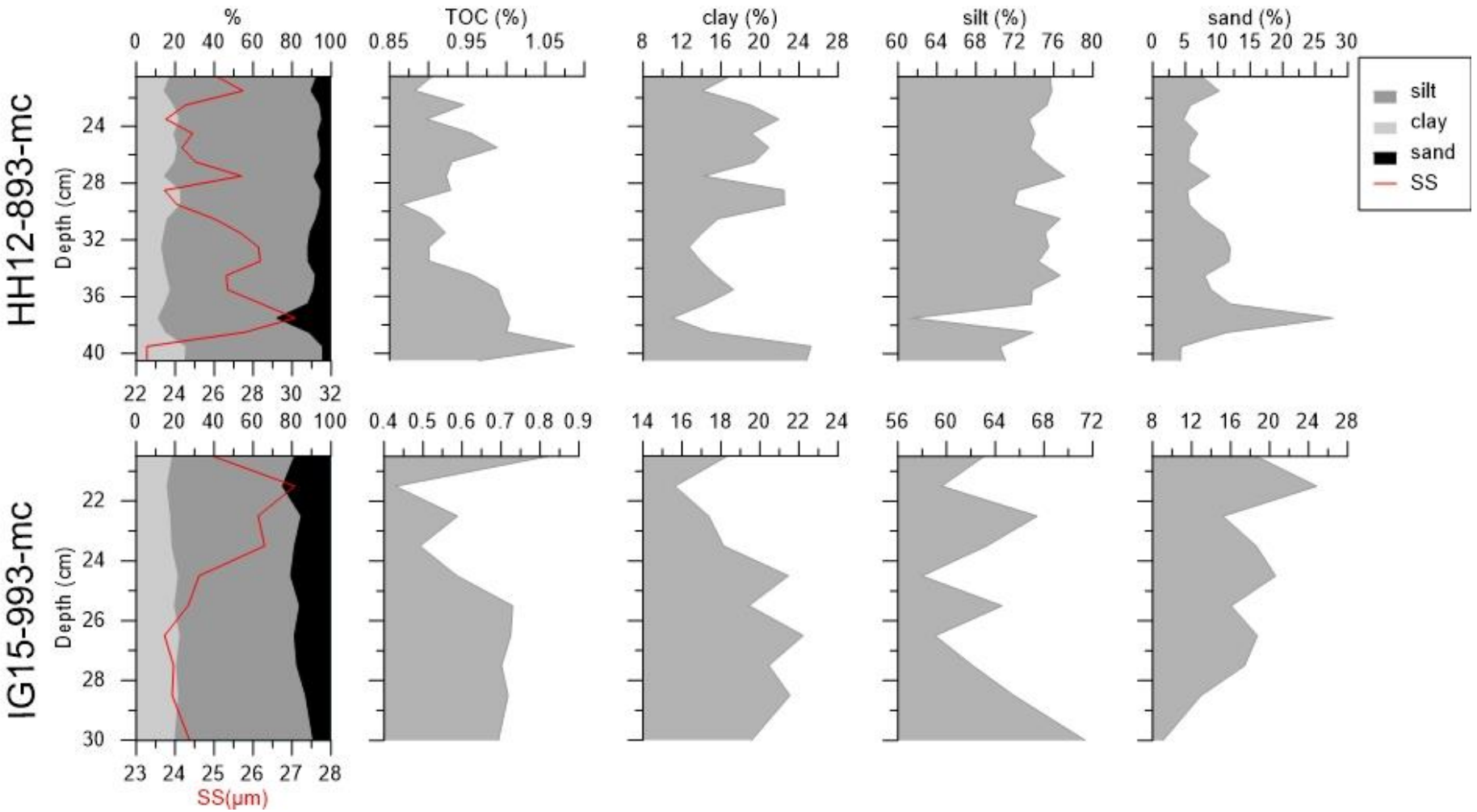

Figure 12: Grain size, TOC and sortable silt results.

4.4 Agglutinated foraminifera

In total six agglutinated species, from a total of 62 species, were identified across the cores (appendix 1). *Reophax* spp. and *Cribrostomoides* spp. were the only agglutinated species with a high enough abundance (>5%), relative to the entire faunal composition, to be mentioned.

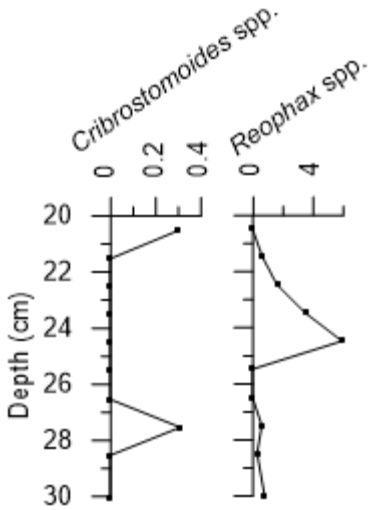

Figure 13: Abundance, relative to the entire faunal composition, in percent, of Cribrostomoides spp. and Reophax spp. in core 993.

In Figure 13, the abundance, relative to the entire faunal composition, of *Cribrostomoides* spp. and *Reophax* spp. in core 993 is shown. The *Cribrostomoides* spp. values never exceed 0.4% for the entire core. *Reophax* spp. has values close to or at 0% from the bottom to 24cm core depth where it increases to 6%. There is a gradual decrease from 6% at 24cm to 0% at the top of the core (Figure 13). The agglutinated flux of the species are generally low, on average 10.4#/cm^2*ka (Figure 18).

In core 893, the abundance, relative to the entire faunal composition, of *Cribrostomoides* spp. is below 1% throughout the core. The *Reophax* spp. is relative stable around 5-10% from the bottom to 34cm, where the abundance increases to about 40%. From 34cm to the top of the core the abundance are generally fluctuating around 30% (Figure 14). The agglutinated flux of the species are generally low, on average 1.6#/cm^2*ka (Figure 18).

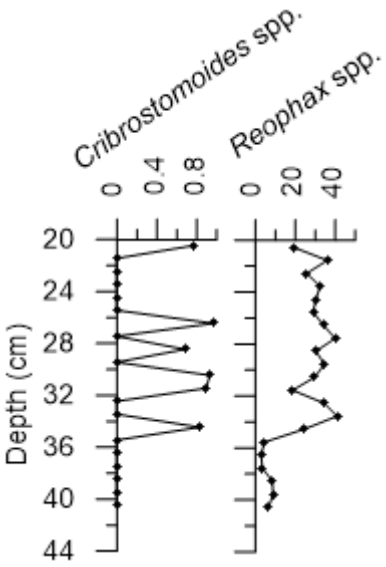

Figure 14: Abundance, relative to the entire faunal composition, in percent, of Cribrostomoides spp. and Reophax spp. in core 893.

A general increasing trend from the bottom to the top of core 897 is observed in the abundance, relative to the entire faunal composition, of *Cribrostomoides* spp. (Figure 15). The abundance of *Reophax* spp. shows a decrease from about 70% at the bottom of the core to about 37cm, where the value stabilizes at around 32%. At 34cm, the value begins to increase to about 60% at 32cm. The abundance stabilizes and is relatively stable up to 28cm where a gradual decrease in the abundance to the top of the core, where it reach below 10% (Figure 15). The agglutinated flux of the species are generally low, on average 4.17#/cm^2*ka (Figure 18).

In core 902, *Cribrostomoides* spp. shows an increase in abundance, relative to the entire faunal composition, from about 5% at the bottom of the core, to a peak of 25% at 38cm. The abundance suddenly drops to around 5% at 36cm, followed by a general increase towards the top of the core where the abundance ends on about 10% (Figure 16). The agglutinated flux of the species in core 902 is the highest of all the cores, on average 76#/cm^2*ka (Figure 18).

The abundance, relative to the entire faunal composition, of *Cribrostomoides* spp. and *Reophax* spp. in core 903 is shown in Figure 17. *Cribrostomoides* spp. are relatively stable around 3% from the bottom of core 903 up to 33cm, where the abundance of *Cribrostomoides* spp. drops to and remain relatively stable around 1% towards the core top. *Reophax* spp. shows a peak of 12% in the bottom, followed by a drop to 3% at 44cm. The abundance remains stable around 3% to the core top (Figure 17). The agglutinated fluxes of the species are higher than for cores 993, 893 and 897, on average 38.5#/cm^2*ka (Figure 18).

As shown in Figure 18, the agglutinated flux is generally lower than the calcareous flux for all the cores. The exception is core 897, below 26cm core depth, where the agglutinated flux is highest. (Figure 18)

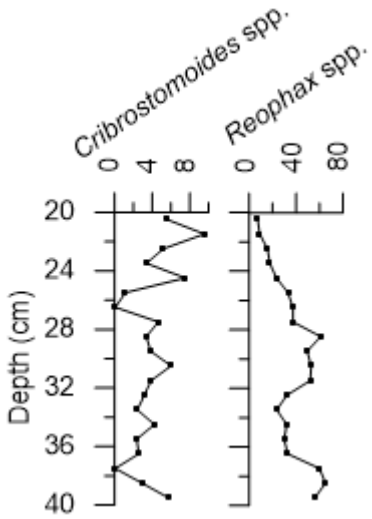

Figure 15: Abundance, relative to the entire faunal composition, in percent, of Cribrostomoides spp. and Reophax spp. in core 897.

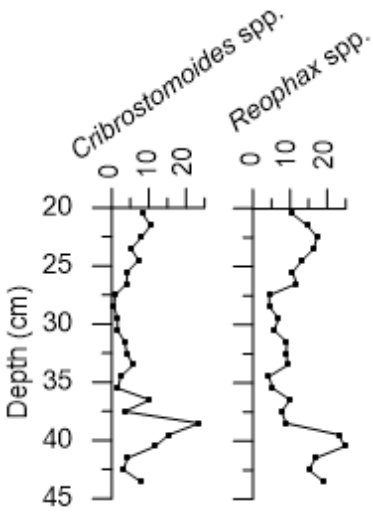

Figure 16: Abundance, relative to the entire faunal composition, in percent, of Cribrostomoides spp. and Reophax spp. in core 902.

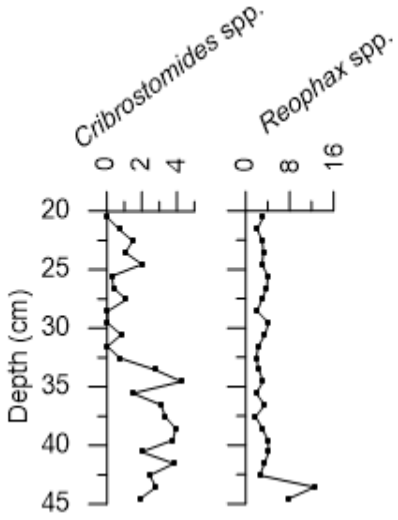

Figure 17: Abundance, relative to the entire faunal composition, in percent, of Cribrostomoides spp. and Reophax spp. in core 903.

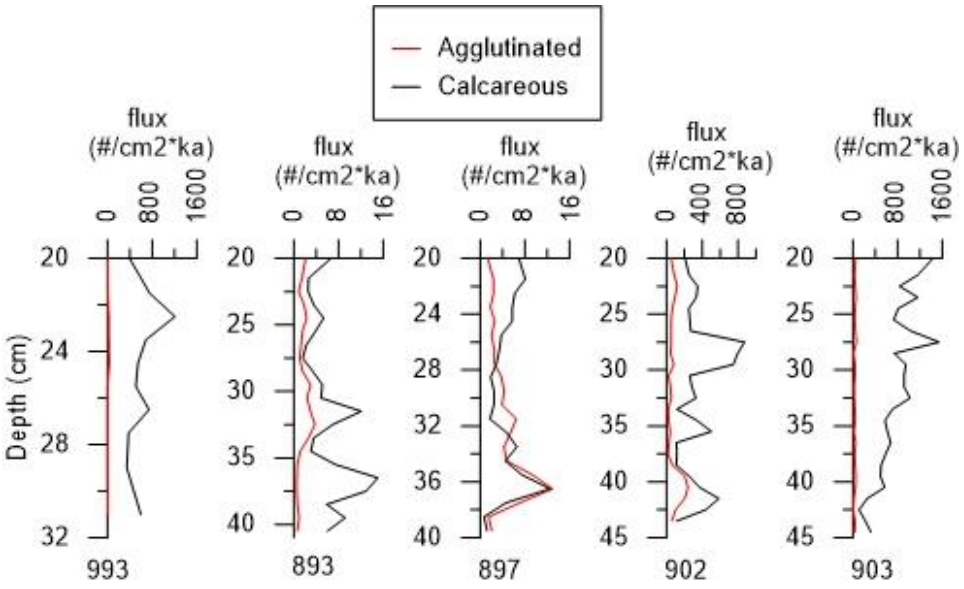

Figure 18: The total agglutinated flux plotted together with the total calcareous flux to give an impression of their relationship.

4.5 Calcareous flux

A constant sedimentation rate is assumed throughout the cores while calculating the calcareous flux. The flux has the unit, numbers per square cm times thousand years (#/cm^2*ka).

4.5.1 HH12-903-mc

The total calcareous flux in core 903 shows a relatively steady increase from the bottom to the top of the core with a bottom value of 101#/cm^2*ka ending in 1321#/cm^2*ka at the top. There is a peak at 27-28cm of 1424#/cm^2*ka, which disturb the stable increasing trend (Figure 18, Figure 19).

4.5.2 HH12-902-mc

In core 902 the total calcareous flux shows fluctuations around 250#/cm^2*ka with an overall stable trend from the bottom to the top. There is an interval between 27cm and 30cm with a higher flux, around 800#/cm^2*ka (Figure 18, Figure 19).

4.5.3 HH12-897-mc

The total calcareous flux values in core 897 is the lowest average flux value of all five cores with an average flux value of 4.7#/cm^2*ka. A peak is present at 36-37cm with a value of 12.5#/cm^2*ka followed by a drop to 4.5#/cm^2*ka at 34cm before a steady increase towards the top, ending on 7#/cm^2*ka (Figure 18, Figure 19).

4.5.4 HH12-893-mc

Core 893 has an average total calcareous flux of 5.9#/cm^2*ka, showing a declining trend towards the top. From the bottom to 30cm the calcareous flux shows fluctuations between 4#/cm^2*ka and 12#/cm^2*ka, followed by a stable period, around 3.5#/cm^2*ka, towards the top (Figure 18, Figure 19).

4.5.5 IG15-993-mc

The total calcareous flux in core 993 shows a relative stable increasing trend towards the top. A general increase is observed from the bottom (~400#/cm^2*ka) to a peak at 22-23cm of 1208#/cm^2*ka before the flux decrease to 400#/cm^2*ka at the top of the core (Figure 18, Figure 19).

Figure 19: Continues on next page.

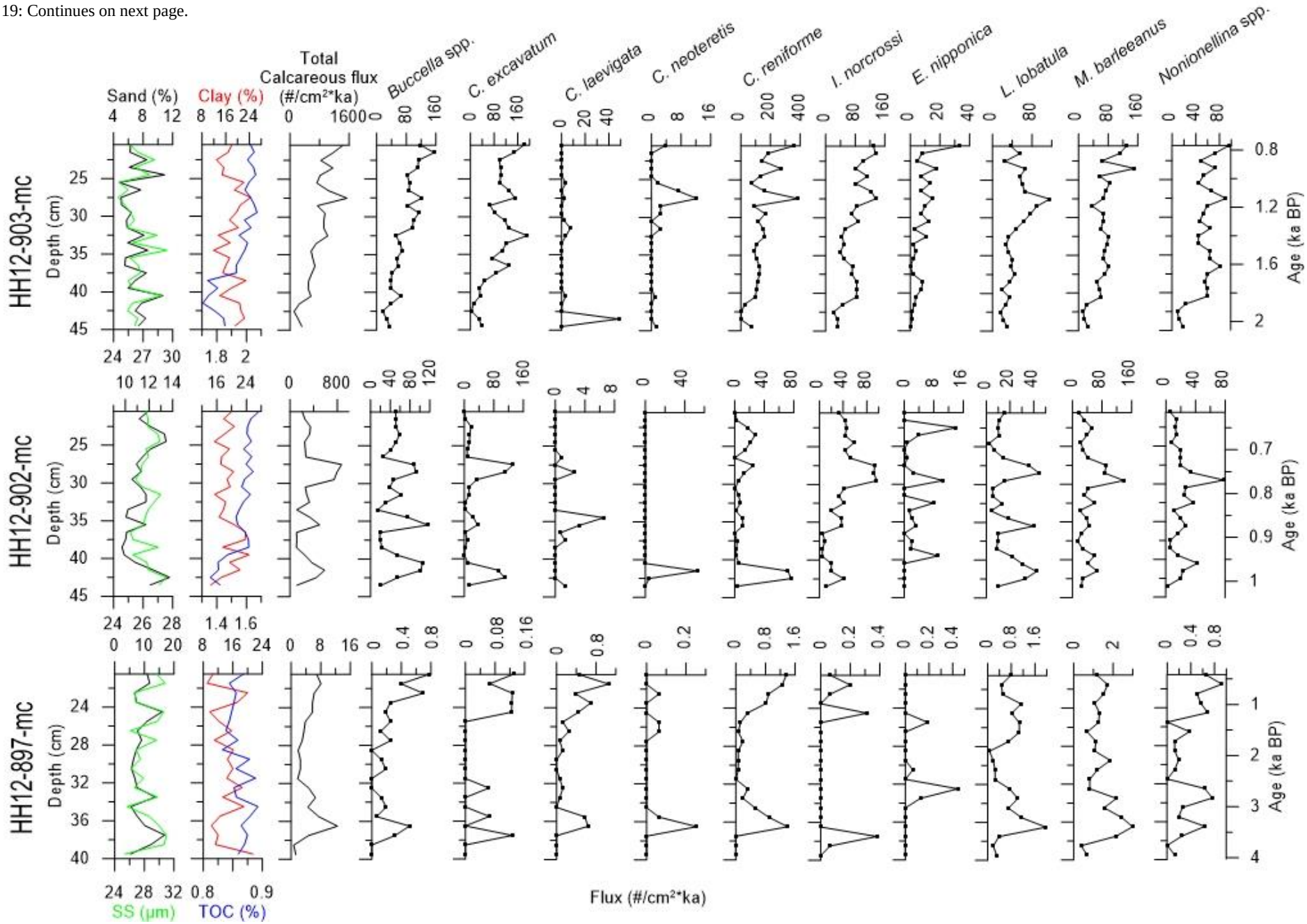

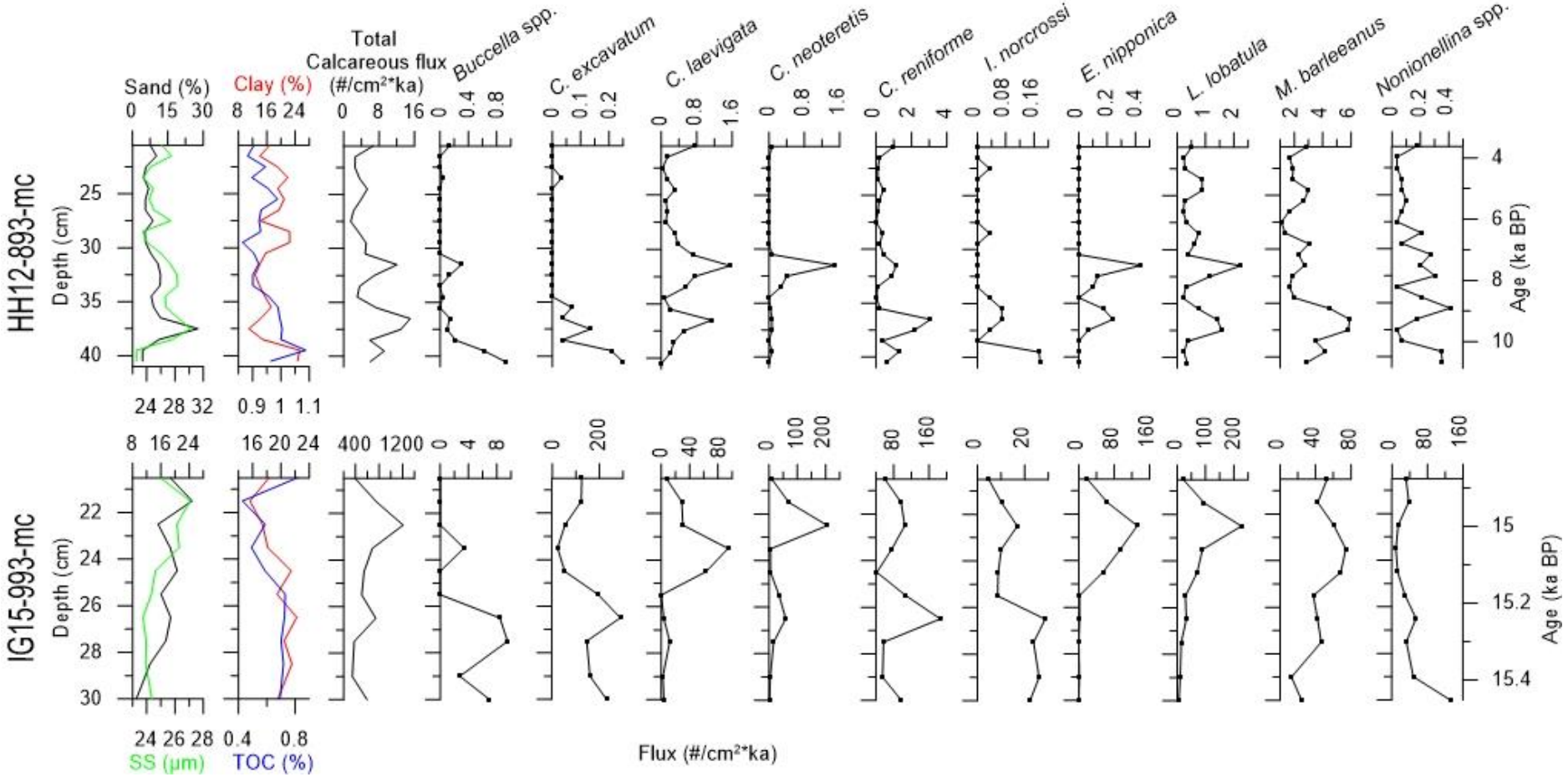

Figure 19: Overview of the flux of the different species. Note the different x-axis scales. It is assumed a constant sedimentation rate throughout the cores for the flux calculations.

4.6 Calcareous species abundance and flux

In total 56 of the 62 identified species were calcareous (appendix 1). The ten most abundant calcareous species in the cores are presented in this chapter. These species were chosen because they show a relative abundance above 5% in at least one sample and are often used in other studies, making is easier to compare results in the discussion section. The relative abundance is calculated only relative to other calcareous species. Changes in flux of the individual species are largely concurrent with changes in relative abundance. Therefore, further mention of flux changes is limited to where they show differences. The cores are described from the bottom to the top.

4.6.1 HH12-903-mc

Buccella spp. fluctuates around 10% with an overall stable relative abundance towards the top of the core. The highest relative abundance of 15% is found as a peak at 41-42cm and the lowest relative abundance of 5% is a low peak at 32-33cm in core 903 (Figure 20).

Both *C. excavatum* and *C. reniforme* show an overall stable relative abundance with fluctuations around 13% and 15% respectively. *C. excavatum* shows a low peak at 42-43cm of 4% before the relative abundance increase to about 13% at 36-37cm. From 36cm to the top of the core, the relative abundance fluctuates around 13% (Figure 20). *C. reniforme* have a similar low peak at 43-44cm where the relative abundance is 0% and show a steady increase to 40cm where it begins to fluctuate around 15% for the rest of the core (Figure 20).

C. laevigata has a low relative abundance of close to or at 0% in core 903. At 43-44cm core depth, there is a peak where the relative abundance is 22% (Figure 20). *C. neoteretis* display a similar pattern as *C. laevigata* with no values above 1% (Figure 20).

I. norcrossi shows a general decrease in relative abundance towards the top of the core. From the bottom of the core to 33cm, the value fluctuates around 15% before a drop to 10% at which the relative abundance continues to fluctuate around towards the top of the core (Figure 20).

E. nipponica has a low relative abundance with an overall increasing trend to the top of the core. From the bottom to 36cm, the relative abundance increase. At 36cm, the value drops 0% before a relatively steady increase towards the top where the relative abundance ends on 2% (Figure 20).

L. lobatula shows a general, relatively stable decrease towards the top of the core. There are two peaks worth noting, one at 42-43cm of 14% and a peak of 12% at 28-29cm core depth (Figure 20).

M. barleeanus shows a relative stable relative abundance trend throughout the core of around 10%, with the exception of the interval between 26cm and 33cm where the value is generally lower and lies relative stable around 6% (Figure 20).

Nonionella spp. has a general decrease in relative abundance from the bottom to the top of the core. The highest value of 11% is observed in the interval between 34cm and 40cm. From 34cm to the top of the core, the relative abundance is relatively stable around 6% (Figure 20).

4.6.2 HH12-902-mc

Buccella spp. shows an overall stable trend around 18% from the bottom to the top of the core. A declining trend is observed from the bottom to 31cm before an increasing trend towards the top of the core (Figure 20).

C. excavatum has an overall average relative abundance of about 6% and appear to have a slightly decreasing trend from the bottom to the top. There are two peaks worth noting at 42-43cm and 27-28cm of 24% and 15% respectively (Figure 20).

C. laevigata has a generally low relative abundance, less than 2%, throughout the core, with an average value of 0.2%. There is an interval of higher values between 35cm and 38cm with an average value of 1.1% (Figure 20).

C. neoteretis shows a relative abundance of 0% from the bottom to the top, with the exception of a peak at 41-42cm of 9% (Figure 20).

The relative abundance of *C. reniforme* shows a relatively stable trend around 2% from the bottom to the top of the core. There are two peaks worth noting, at 42-43cm and 23-25cm with values of 17% and 8% respectively (Figure 20).

I. norcrossi shows a fluctuating, but general increasing relative abundance from the bottom to the top of the core starting at 5% ending on 15% (Figure 20). The same trend is observed for the *I. norcrossi* flux with the exception of an interval with a peak in the flux values between 27cm and 30cm (Figure 19).

E. nipponica does not show any apparent trends and the relative abundance is less than 4%. There are two peaks with values close to 4% at 39-40cm and 22-23cm (Figure 20).

L. lobatula has an overall decreasing trend towards the top of the core. At a core depth of 35cm, a drop in the relative abundance, from an average value of 8% to an average value of 3.5%, is observed (Figure 20). *L. lobatula* shows a similar trend in the flux, with the exception of an interval with lower values between 36cm and 39cm (Figure 19).

M. barleeanus fluctuates between 10% and 20% with an overall stable relative abundance towards the top of the core. The fluctuations show a trend of lower amplitudes towards the top of the core (Figure 20).

Nonionella spp. shows an overall stable trend with increasing relative abundance from the bottom to 30cm (from 4% to 10% respectively), where the value drop and remains relatively stable around 5% towards the top (Figure 20).

4.6.3 HH12-897-mc

The relative abundance of *Buccella* spp. fluctuates, but shows a general increase from the bottom to the top of the core from about 4% to 8% (Figure 20).

C. excavatum does not show any values above 3% and have an overall stable calcareous abundance from the bottom to the top of the core. However, there are two peaks, one at 37-38cm and another is an interval at 22-25cm with a relative abundance of 2.7% and 2% respectively (Figure 20).

C. laevigata shows a relative abundance fluctuating around 8% with an overall increasing trend towards the top of the core. There is a peak at 35-36cm of 7.7% (Figure 20). This is the same pattern as observed in the *Buccella* spp.

C. neoteretis has a general low relative abundance in core 897 with values less 2% not showing any obvious trends. However, there are two peaks at 36-37cm and 25-27cm with values of 2% and 1.7% respectively (Figure 20).

C. reniforme shows a general increase in relative abundance from the bottom to the top of the core. An interval with higher values is observed at 34-37cm depth with a value of above 11%. The observed increase mainly occurs from 26cm towards the core top (Figure 20).

I. norcrossi has a relative abundance close to or at 0% for the most of the core. There are two peaks at 24-25cm of 5% and 37-39cm of 9% (Figure 20).

E. nipponica mostly shows a relative abundance at or close to 0% with the exception of two peaks at 32-33cm and 25-26cm of 9% and 5% respectively (Figure 20).

L. lobatula shows a slight overall decreasing relative abundance. There is a decreasing trend from the bottom to 27cm (from 15% to 3%) where a shift to higher relative abundance (31%) occurs before a relatively steady decline towards the top of the core, ending on 11% (Figure 20). A similar trend is observed in the *L. lobatula* flux, with the exception of a high peak at 36-37cm (Figure 19).

M. barleeanus display an overall decreasing trend from the bottom to the top of the core from 50% to 17%. There is a major peak worth noting at 29-30cm of 74% (Figure 20). The *M. barleeanus* flux shows a similar trend, with slightly higher values towards the bottom, before a sudden drop (Figure 19).

Nonionella spp. fluctuates between 0% and 15% throughout the core, with an overall increasing trend. There is a high peak at 32-33cm of 13% and a low peak at 25-26cm of 0% that disturbs the general increasing trend (Figure 20).

4.6.4 HH12-893-mc

Buccella spp. shows a relative abundance close to or at 0% throughout the core. The only exception is a peak at the bottom of the core of 15% (Figure 20).

C. excavatum shows a similar trend as *Buccella* spp. with a relative abundance below 5% (Figure 20).

C. laevigata shows some fluctuations, but have a slight increase in relative abundance from the bottom and up. There is an interval of higher values around 13% between 30cm and 34cm (Figure 20).

C. neoteretis has values close to or at 0% throughout the core, with the exception of a peak similar to the interval with higher values for *C. laevigata* at 31-33cm of 7-12% (Figure 20).

C. reniforme shows a fluctuating relative abundance around 10% with an overall decreasing trend towards the top. There is one peak worth noting at 36-37cm of 20% (Figure 20).

I. norcrossi have generally low relative abundance values less than 3%. The highest values are found in the bottom of the core, close to 3% (Figure 20).

E. nipponica has the highest relative abundance from the bottom up to 31cm, with the highest value of 3.6%. At 31cm the value drops to 0% and remain there towards the top of the core (Figure 20).

L. lobatula shows a fluctuating relative abundance between 5% and 25% with an overall increase towards the top of the core. The amplitude of the fluctuations becomes greater up core (Figure 20).

M. barleeanus has a fluctuating relative abundance with a slight overall increasing trend from the bottom to the top. There is a low peak at 31-32cm of 22%, which is the lowest value in the core and dilutes the signal of an overall increasing trend. The highest value in the core is 75% and is found at 22-23cm (Figure 20). The *M. barleeanus* flux shows an opposite trend from the relative abundance. In the same area as the relative abundance show an increase, the flux shows a decrease (Figure 19).

Nonionella spp. shows a fluctuating relative abundance with an overall decreasing trend towards the top. The values are not exceeding 7%. There is a shift from high amplitude fluctuation between 1% and 7% in the bottom to a relative stable relative abundance around 1.8% at 27cm (Figure 20).

4.6.5 IG15-993-mc

Buccella spp. has a relative abundance of less than 5% and the trend is relative stable throughout the core. There is a peak at the top of the core of 5%, other than that the value is generally between 0% and 2% (Figure 20).

C. excavatum has a decreasing relative abundance towards the top. The value is relative stable around 38% in the bottom and at a depth of 25cm, the value drop to 9% before a relatively steady increase towards the top where it ends on 31% (Figure 20).

C. laevigata shows a fluctuating relative abundance with an overall stable trend from the bottom to the top of the core. There is an interval between 23cm and 25cm with higher relative abundance where the value is around 12% (Figure 20).

C. neoteretis has an increasing relative abundance towards the top of the core. There is an interval of values under 1% between 23cm and 25cm, which dilutes the increasing trend. A high peak is found at 22-23cm with a value of 17% before decreasing towards top of the core (Figure 20).

C. reniforme shows a slight decrease in relative abundance from the bottom to the top of the core. The value is relative stable from the bottom to 25cm, where the relative abundance drops from 20% to 8% before a steady increase towards the top (Figure 20).

I. norcrossi has a general decrease in relative abundance from the bottom towards the top of the core. The relative abundance is at its highest in the bottom of the core (6%) before a steady decrease to 1.7% at 26-27cm where the value remain relatively stable for the rest of the core (Figure 20).

E. nipponica shows an increasing relative abundance towards the top of the core. The value lies steadily at or close to 0% from the bottom up to 25cm where the value increase and reach the highest value of 13.7% at 23-24cm before decreasing towards the top (Figure 20).

L. lobatula shows a similar trend in calcareous abundance as *E. nipponica*, with low relative abundance values from the bottom up to 25cm before an increase reaching a high value of 18% at 22-23cm before decreasing towards the top (Figure 20).

M. barleeanus shows fluctuating relative abundance around 8%, with an overall increasing trend towards the top (Figure 20).

Nonionella spp. has a relative stable relative abundance, with an overall decreasing trend towards the top of the core. The bottom and top values are 21.8% and 7.8% respectively (Figure 20).

Figure 20: Continues on next page.

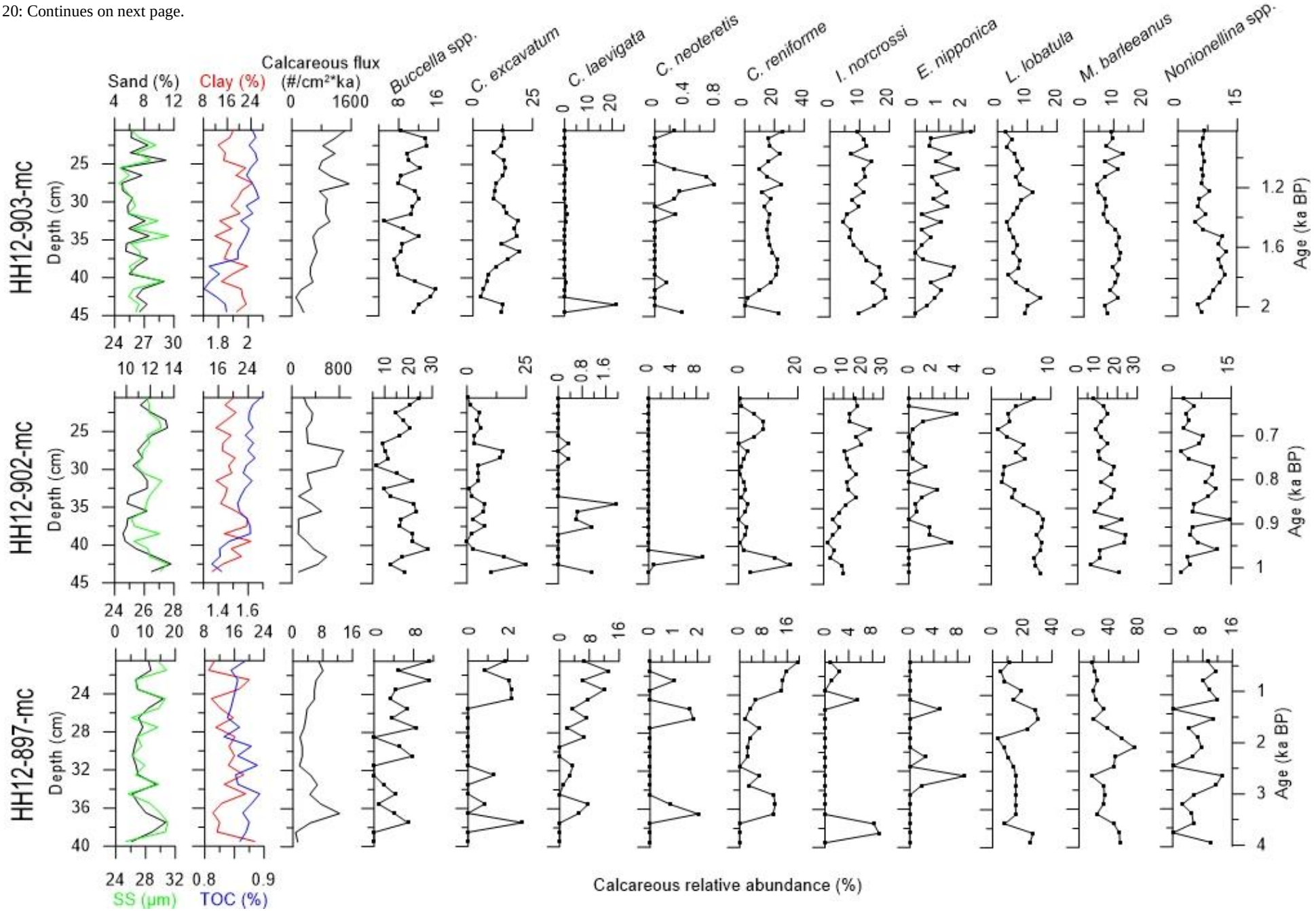

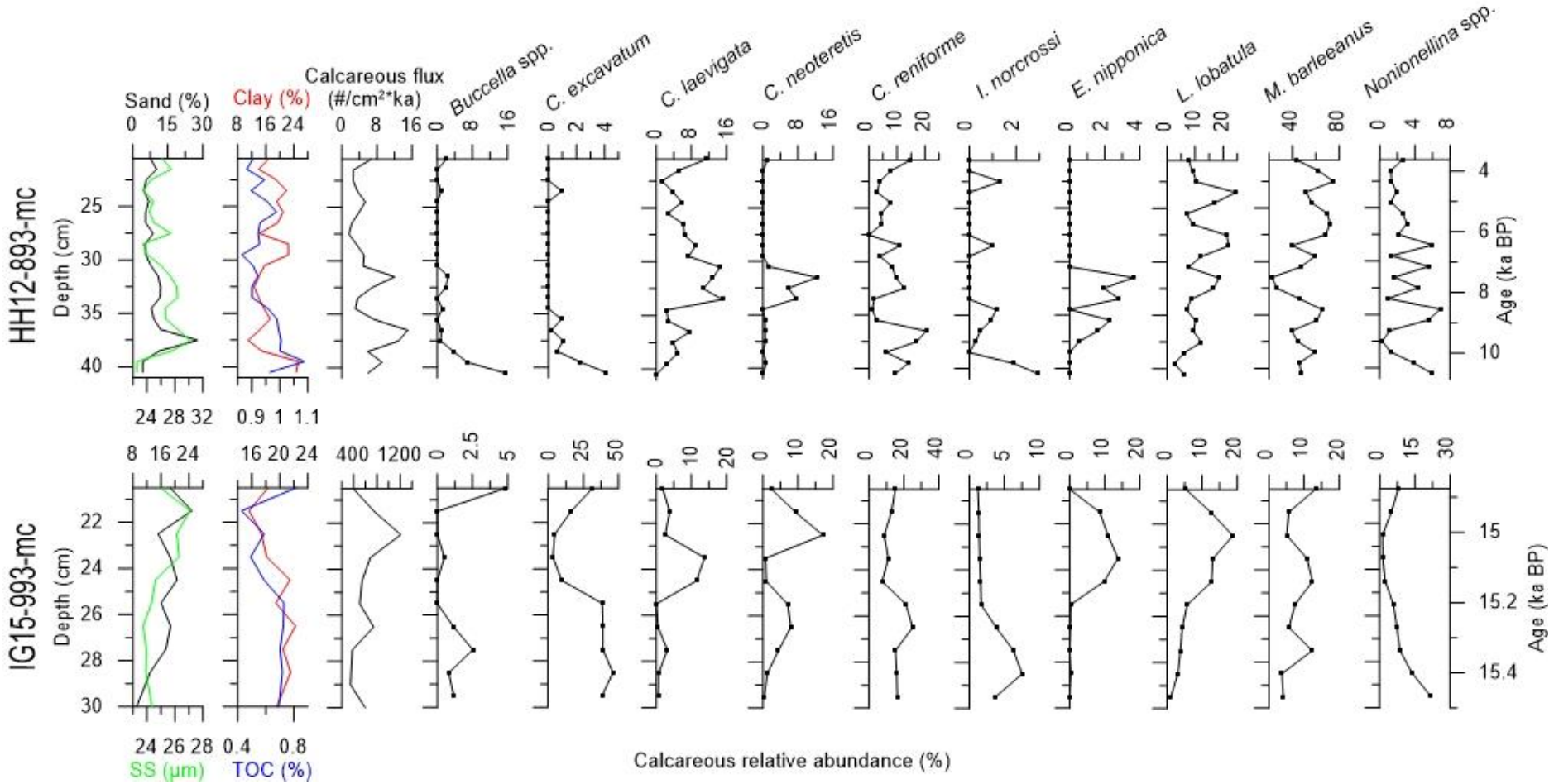

Figure 20: The relative abundance of the ten most common calcareous species for all five cores. Sortable silt (SS), sand, clay, total organic carbon (TOC) and the calcareous flux are shown to the left in the figure. Notice the different x-axis scales.

5 Discussion

This section includes an interpretation and a discussion of the results from the previous section.

The variation in the inflow of Atlantic water is discussed using results obtained in this study compared to previous studies on Atlantic water inflow on the Barents Sea region. To provide a good overview and easier comparisons, the discussion is divided into four time intervals based on significant changes in the fauna observed in the dataset. The time intervals covered by the cores represent the Late Glacial (15 500-14 900yr BP), early Holocene (10 900-7300yr BP), mid Holocene (7300-2500yr BP) and late Holocene (2500-400yr BP). The start of the Holocene is widely accepted as 11 700yr BP, and the period is often sectioned in the early (11 000-7500yr BP), mid (7500-2500yr BP) and late (2500-0yr BP) Holocene (Risebrobakken, et al., 2010), although different authors may use different ages depending on their sampled data. All ages are, where possible, rounded off to nearest hundred calibrated years before present due to the error margins of the datings.

The calcareous flux in core 897 and 903 show a similar pattern, both show an increase in flux starting about 2000yr BP towards the present. Core 902 covers a smaller portion of the period, thus giving a more detailed view on the flux changes, making it hard to fit to the other two northern cores (Figure 19). Core 893 is the core covering the longest time span with the lowest average sedimentation rate. Both core 902 and 903 show some overlapping with each other and core 897 cover the entire time span of both those cores as well as a part of the youngest age of core 893 (Figure 8). Core 993 is not overlapping with any of the other cores in this study.

Improved environmental conditions are in this thesis defined as a warmer environment with higher food availability, unless otherwise stated in the text.

The TOC in the southwestern Barents Sea is mainly composed of marine organic material originating from nutrient rich Atlantic water (Knies & Martinez, 2009). During spring bloom, there is a high vertical export of phytoplankton and incomplete degradation of the organic material, due to high productivity. This might explain the enrichment of organic material in the sediments (Knies & Martinez, 2009). These blooms are an important food source for benthic foraminifera, and since they may occur as a result of the inflow of nutrient rich

Atlantic water, the variability in the inflow therefore influence the benthic foraminiferal assemblages (Knies & Martinez, 2009). Phytoplanktic blooms may also occur in proximity of a sea ice edge or marginal ice zone (MIZ) and at the Arctic Front (Slubowska, et al., 2005; Knies & Martinez, 2009).

C. reniforme, C. excavatum and *Nonionella* spp. show high relative abundance, especially in core 903, supporting a colder and possibly a sea ice or front proximal environment. TOC has a reduced preservation potential in coarse-grained sediments relative to finer sediments, as the fine-grained sediments might reduce exposure to oxygen, and bind the organic matter to clay particles, thus preserving the organic material better (Hald & Steinsund, 1992; Kennedy, et al., 2002).

The sortable silt correlates well with the sand content in all cores, except from core 993, where the sortable silt and sand values show opposing trends. Due to the late glacial age of core 993, and influence from IRD (Figure 9), $\Delta\overline{SS}$ was calculated (Figure 11).

Descriptions of the environmental preferences of the different species are given in section 2.5 Ecological preferences.

5.1 Agglutinated flux

The agglutinated species *Cribrostomoides* spp. and *Reophax* spp. are generally displaying a low flux in all the cores (Figure 18). The highest flux (239.5#/cm^2*ka) of agglutinated species is found in core 902 at 40-41cm core depth. The high abundance, relative to the total fauna, of *Reophax* spp. in core 897 and 893 might be due to *Reophax* spp. being tolerant to poor trophic conditions and adapted to low amounts and poor quality of organic material (Dessandier, et al., 2015). The intervals in core 897 where the agglutinated flux is higher than the calcareous flux might be explained by the generally low (<16#/cm^2*ka) flux throughout the core (Figure 18), as *Reophax* spp. is an opportunistic species, capable of surviving where other species struggle (Dessandier, et al., 2015). The higher presence of *Reophax* spp. in the top of core 993 corresponds with higher current strength inferred by $\Delta\overline{SS}$ (Figure 11D, Figure 13).

Dense and saline water (brine) is often found in association with areas with sea ice formation, such as a sea ice edge and Arctic Front (Steinsund & Hald, 1994). Brine formation at the Arctic Front, sea ice edge or in an area covered by sea ice may cause the seawater to contain a higher amount of CO_2 than the surrounding water (Steinsund & Hald, 1994). As brine is

denser than the surrounding seawater, it sinks to the sea floor, bringing the CO_2, making the bottom water more acidic (Steinsund & Hald, 1994). In addition to transporting CO_2 to the sea floor, the downward current caused by the sinking brine creates well oxygenated conditions at the sediment-water interface, which can cause oxidization of organic material and produce even more CO_2 (Steinsund & Hald, 1994). Acidification of the bottom water can cause dissolution of the calcium carbonate tests of calcareous benthic foraminifera. The dissolution mainly occurs on epifaunal species as sediments cover the infaunal species thus they have better protection against the dissolution (Steinsund & Hald, 1994). Steinsund & Hald (1994) found a correlation between higher values of agglutinated species and low amounts of calcium carbonate, suggesting higher values of agglutinated species in areas dissolution of calcium carbonate occur (Steinsund & Hald, 1994).

Dissolution of calcareous species might explain the high agglutinated flux relative to the calcareous flux in the cores 893 and 897 (Figure 18). As the CCD generally appears at depths greater than 4500m (Allaby, 2013) it is more likely that brine, enriched in CO_2, is the source of the possible dissolution.

The agglutinated foraminifera have not been further elaborated in this thesis as it is a known fact that agglutinated foraminifera have a poor preservation potential down core (Slubowska, et al., 2005; Dijkstra, et al., 2015; Sejrup, et al., 2004) and the agglutinated flux is generally low (Figure 18). For this reason, to avoid erroneous low relative abundances of calcareous species in Figure 20, the relative abundances are based on the calcareous taxa only, unless stated otherwise in the text.

5.2 The Late Glacial (15 500-14 900yr BP)

Core 993 is not compared with the other cores due to the age difference, where the top of core 993 is dated to 14 900yr BP and the closest core, in distance and age, core 893, begins at 10 900yr BP (Figure 8, Table 4). The 4000yr time gap is considered too large to allow a direct comparison between the cores.

The TOC value shows the same down core pattern as the Arctic species *C. excavatum*, which is associated with Arctic and glaciomarine environments (Mackensen, et al., 1985; Hald, et al., 1994). An explanation for the correlation between TOC and *C. excavatum* can be higher primary production at a marginal ice zone, providing more organic material to the seafloor between 15 400yr BP and 15 100yr BP (Figure 20) (Knies & Martinez, 2009). Additionally,

the TOC and clay values correlate well throughout the core, indicating a connection in the controlling factors of TOC and clay content. This corresponds to the findings of e.g. Dijkstra et al. (2015), Junttila et al. (2014) and Groot et al. 2014, that TOC show a good correlation with clay, as both clay and organic material show absorptive properties (Kennedy, et al., 2002).

The increasing sand content might indicate stronger currents at core 993, which transport organic material as well as finer sediments, away from the site, leaving a higher observed sand content. The observed sand would then be a lag deposit from winnowing, a process where the current sort out and transport the fine grained sediments away from the site (King, et al., 2014). The overall increasing presence of sand and *L. lobatula* and the decreasing content of clay and TOC supports an increase in hydrodynamic activity, which could explain the different sources of the sand and sortable silt discovered when calculating $\Delta\overline{SS}$ (Figure 11, Figure 20). The increase of $\overline{SS}$ and the calculated $\Delta\overline{SS}$ supports stronger currents for the most recent parts of core 993 (Figure 11). It is reasonable to assume that an increase in hydrodynamic activity at core 993 may have caused reworking of the sediments present, and deposit already reworked sediments.

The overall increasing presence of *C. laevigata, C. neoteretis, E. nipponica* and *M. barleeanus* (Figure 20), all associated with Atlantic or Atlantic derived water, together with the decrease of *C. excavatum, C. reniforme* and *I. norcrossi*, associated with colder conditions (Figure 20), can indicate a warmer and/or more nutrient rich Atlantic water influenced environment (Dijkstra, et al., 2015) towards 14 900yr BP. This foraminiferal assemblage could reflect the beginning of the retreat of the Scandinavian ice sheet from its late Weichselian maximum position at 17 000-15 000yr BP (Mangerud, et al., 2004). About 15 000yr BP the lobe area of Ingøydjupet was ice free (Ruther, et al., 2011), indicating open water over the southern parts of the southwestern Barents Sea and likely over core 993.

At 15 300yr BP the first signs of a warming appear, where *C. excavatum, C. reniforme* and *I. norcrossi* begin to decrease, shortly followed by an advance of *C. laevigata, E. nipponica* and *L. lobatula* at 15 200yr BP (Figure 20). The advance of the warm water species *E. nipponica*, associated with warm Atlantic bottom water (Saher, et al., 2012), and disappearance of the cold water species C. *excavatum*, associated with Arctic conditions (Mackensen, et al., 1985), suggests a period of stronger Atlantic water inflow. This is further supported by the increase of the *M. barleeanus* flux (Figure 19), which is associated with Atlantic derived waters

(Mudie, et al., 1984). Both clay and TOC show a decrease from 15 200yr BP, the same time the *M. barleeanus* flux increase, suggesting another factor controlling the increasing flux of *M. barleeanus*. As *M. barleeanus* prefers partially degraded organic material, often redeposited from shallower areas (Caralp, 1989), it could be that the organic material is redeposited from a nearby shallow bank, such as Tromsøflaket. Due to the simultaneously increase in the flux of *C. laevigata*, associated with Atlantic water (Klitgaard-Kristensen, et al., 2002), it is likely the area was influenced by Atlantic derived bottom water around 15 200yr BP.

The indications of Atlantic water inflow last until 15 000yr BP where *E. nipponica* and *L. lobatula* start to disappear and *C. excavatum* begins to advance. *C. laevigata* disappears earlier (15 100yr BP) than the two other species and is replaced by a suddenly appearance of *C. neoteretis* which begins to decrease almost immediately after. This can be interpreted as a cooling of the Atlantic bottom water, considering *C. neoteretis* prefer chilled Atlantic water and organic rich sediments (Mackensen & Hald, 1988). Organic rich sediments may occur as a result of phytoplanktic blooms, often associated with Atlantic water, in connection with a seasonal sea ice edge or at the Arctic Front (Knies & Martinez, 2009), thus possible indicating an advance of the Arctic Front towards the core site bringing cooler conditions or a cooling of the incoming Atlantic water.

The flux peak at 15 000yr BP is mainly caused by an increase in the flux of *C. neoteretis, E. nipponica* and *L. lobatula*. This could be due to a strong inflow of Atlantic water, transporting the readily reworked *E. nipponica* (Saher, et al., 2012; Hald & Steinsund, 1992; Murray, et al., 1982) to core 993, reflected in the increased sortable silt mean grain size. At the same time, there is a low peak in the sand concentration. The low peak is not necessarily due to a decrease in sand concentration, but rather an increase in the silt and clay fractions. The stronger current may have transported and redeposited the tests of *E. nipponica* to the site, as its small and round shape makes it more susceptible for reworking (Murray, et al., 1982; Hald & Steinsund, 1992; Saher, et al., 2012), thus giving a false impression of the actual abundance of *E. nipponica*.

The poor correlation between measured $\overline{SS}$ and $\overline{SS}_{\text{pot}}$ (Figure 11C) indicates different transportation and deposition processes between the sortable silt and sand, suggesting the silt is not ice rafted. The $\Delta\overline{SS}$ show a higher current strength than what is to be expected towards the top of core 993 (Figure 11D), which correlates well with the occurrence of *L. lobatula*.

The high current strength could be the reason for the obtained low sedimentation rates, as mud and possibly some foraminifera can be transported away from the site, by winnowing, hence the low (19.1cm/ka) sedimentation rates at core 993. It is also possible that the higher bottom current speeds, inferred by the $\Delta\overline{SS}$ calculations, have transported some old material and foraminifera from nearby areas, contributing to the old datings.

In addition, another species associated with strong bottom currents, *Trifarina angulosa* (Hald & Steinsund, 1992), not mentioned earlier due to its small relative abundance in most of the cores, show the same trend as *L. lobatula*, thus supporting a strong hydrodynamic environment at the time.

A significant amount of IRD (Figure 9) was observed when sieving the samples, indicating the presence of icebergs. This is also one of the reasons for calculating $\Delta\overline{SS}$, to investigate if the sand, assumed ice rafted, and $\overline{SS}$ originates from the same source. The amount of IRD suggests icebergs drifting over the core site, supporting the suggestion of a retreat of the Scandinavian ice sheet, described by Mangerud et al. (2004). A high IRD content was also observed further south by Klitgaard-Kristensen et al. (2001) in the period 18 000- 14 499yr BP. They suggest the high IRD content indicate a harsh environment, strongly influenced by glaciers and outlet of icebergs (Klitgaard-Kristensen, et al., 2001).

The general trend during the Late Glacial, here represented by core 993 (15 500-14 900yr BP), is a high relative abundance of both *C. excavatum* and *C. reniforme*, suggesting a cold and possibly a glacial proximal, or near a glacier, in the early parts. A general warming trend follows towards the Holocene, as inferred by the increasing flux of *M. barleeanus*, *C. laevigata*, *C. neoteretis* and *E. nipponica* (Figure 19). Slubowska-Woldengen et al. (2008) found similar results, showing a warming trend in the southeast Barents Sea.

Although it is possible to obtain results from core 993, due to the old age and the chance of the core being partly reworked the results are potentially less reliable, and care should be taken interpreting the core.

5.3 Early Holocene (10 900-7300yr BP)

The early Holocene is covered by the bottom half of core 893 (10 900-7300yr BP). The area of core 893, in the southwestern Barents Sea, is dominated by *M. barleeanus* in the beginning and middle parts (10 900-8700yr BP) of the early Holocene, rapidly replaced by *C. laevigata*

and *L. lobatula* towards the end of the mid- early Holocene, 8700yr BP. An initial decrease, from 10 900yr BP, in the Arctic species *C. excavatum*, *C. reniforme* and *I. norcrossi* could indicate the end of a cold period, and the beginning of a period with a warmer environment. Northwest of core 893, in Kveithola trough, a similar decrease of arctic foraminifera is observed during this time (Groot, et al., 2014). The decreasing Arctic species are replaced by an increase in the relative abundance of *C. laevigata*, *E. nipponica* and a high relative abundance of *M. barleeanus* (Figure 20). This may suggest a warming of the bottom water, causing an improvement of environmental conditions for the species associated with warmer, more nutrient rich water, possibly as a response to an increase in the inflow of Atlantic water.

C. reniforme occur in high abundance (>10%) between 10 900yr BP and 9100yr BP. However, the abundance of *C. reniforme* is not stable enough on a high abundance to be called a dominant species in the southwestern Barents Sea during the early Holocene (Figure 20). The general increase in *E. nipponica* and *C. laevigata* (Figure 20) suggest warmer bottom water passing over core 897 in the middle and late parts (8700-7300yr BP) of the early Holocene, indicating an increased inflow of Atlantic water in the middle and late parts of the early Holocene. Slubowska-Woldengen et al. (2008) observed similar trends with inflow of Atlantic water to the southeastern Barents Sea via the NCaC, together with a general dominance of *M. barleeanus* and *C. reniforme* in the southeast Barents Sea during the early Holocene (9500-7500yr BP (Slubowska-Woldengen, et al., 2008)). This supports the findings in this study, of a general warming trend during the early Holocene.

The general dominance of *M. barleeanus* and *L. lobatula* occasionally supported by *C. reniforme* suggests a strong influence of Atlantic water and stronger bottom current speeds (Hald & Steinsund, 1996; Mackensen, et al., 1985). The continuous presence of *C. laevigata* and *Nonionella* spp. also point towards a stronger influence of Atlantic water over core 893 throughout the early Holocene. The high sand concentration (28%) and sortable silt (30µm) at 9800yr BP corresponds to the peaks in the flux of *M. barleeanus* and *L. lobatula* (Figure 19). As little to no IRD (Figure 9) were found during sieving it is unlikely the increased sand and sortable silt originates from icebergs or sea ice (Gilbert, 1990). Due to the lack of IRD and the peak in *L. lobatula*, it is suggested that stronger bottom currents, removing the clay particles (winnowing), is the reason for the observed increase in sand concentration, rather than an increase in deposited sand.

The decrease in the relative abundance of *M. barleeanus* towards the end of the early Holocene is not reflected in the *M. barleeanus* flux, which remain stable for the late early Holocene. This indicates an increased flux of other species rather than a decrease of the presence of *M. barleeanus* (Figure 19, Figure 20).

Almost all the foraminifera species in core 893 show fluctuations with an increasing trend for both flux and abundance in the period 10 900yr BP to 7300yr BP. This may suggest an unstable and shifting inflow of Atlantic water during the early Holocene. The total calcareous flux is generally low (<16#/cm^2*ka), thus small changes in a species flux has a great impact on the relative abundances. However, the observed foraminiferal faunal composition, mainly consisting of *C. laevigata, E. nipponica, L. lobatula, M. barleeanus* and *Nonionella* spp., suggests a general warming.

5.4 Mid Holocene (7300-2500yr BP)

The disappearance of *E. nipponica, C. neoteretis* and a decline of *C. laevigata* together with the stabilizing low flux (<2#/cm^2*ka) of *L. lobatula* and *M. barleeanus* from 7300yr BP, can indicate a shift to a cooler environment towards the top of core 893. The increased and stable clay content from 6000yr BP suggest a calm environment. The total flux decrease at the same time, and remain stable at a low value (3-8#/cm^2*kyr) for the rest of core 893 (Figure 19).

A period with a calmer environment is observed in core 893 between 7300yr BP and 6900yr BP as indicated by an increase in clay content and decrease in the silt fraction together with a small decrease in sand concentration. The sortable silt shows a decrease as well, indicating a decrease in the coarse silt fraction. The TOC concentration is lower at 7300yr BP, but show an increase to 6900yr BP, when the clay content is high. Around the same time, the relative abundance of *C. laevigata* declines and *C. neoteretis* disappear, possibly as a consequence of change in the physical environment, as they are limited by fine grain sediments (Mackensen & Hald, 1988; Mackensen, et al., 1985). This increase of finer particles correlates well with the increase of *M. barleeanus*, further supporting that changes in the physical environment is the main controlling factor of the foraminiferal species assemblage. *L. lobatula* continue with a generally increasing relative abundance, however, the fluctuations increase in both amplitude and period. The *L. lobatula* flux becomes relative stable, indicating the shifting abundance to be caused by variations in other species rather than for *L. lobatula*. The increasing clay content may suggest weaker currents, and together with a decline in species

associated with Atlantic water, such as *C. laevigata* and *C. neoteretis*, this indicates a reduction in the inflow of Atlantic water.

The pulses of higher relative abundance of *Nonionella* spp. from 7300yr BP to 6000yr BP and the lack of other species associated with sea ice and fronts, suggest the pulses of *Nonionella* spp. to be caused by changes in food supply (Jennings, et al., 2011), rather than a seasonal sea ice cover or a front. This is supported by the low and stable TOC values around 6000yr BP, the same time the relative abundance of *Nonionella* spp. stabilize at a lower value. The stabilizing, higher clay concentration at 6000yr BP, and the lower sand concentration, supports a calmer environment in the mid Holocene.

The overall declining trend of the total calcareous flux from the early Holocene in core 893, stabilize at low values (<8#/cm^2*ka), starting at 7300yr BP to the top of core 893 (3600yr BP), suggesting a low food availability in the area during the mid Holocene. This is reflected in the TOC values, which follows the trend of the flux (Figure 19).

The generally increasing, yet fluctuating relative abundance of *L. lobatula* in core 893 may indicate an increasingly unstable hydrodynamic activity between 7300yr BP and 3600yr BP. This trend is also reflected in the relative abundance of *M. barleeanus* which show an opposite trend, when the relative abundance of *M. barleeanus* increase, the relative abundance of *L. lobatula* decrease and vice versa (Figure 20). The indications of increasingly hydrodynamic activity, inferred by *L. lobatula*, is not supported by the grain size distribution suggesting another controlling factor of the increase in *L. lobatula*, such as food availability or salinity (Hald & Steinsund, 1996).

The flux of *L. lobatula* and *M. barleeanus* remains relatively stable from 7300yr BP towards the core top, thus indicating a reduction in other species rather than increasing favorable environmental conditions for *L. lobatula* and *M. barleeanus*. This suggests relatively calm and stable environmental conditions during the mid Holocene (7300-2500yr BP), which is indicated by the relatively stable grain size distribution. The TOC is relative stable around 0.9% and shows the higher values at the same time *M. barleeanus* show highest flux and relative abundance (Figure 19, Figure 20).

The generally low total flux (3-12 #/cm^2*kyr) observed between 7300yr BP to 2500yr BP, seen in cores 893 and 897, might suggest a period of low primary productivity, providing fewer nutrients to the sea floor. This is also apparent in the lower (<1%) TOC values in both

cores 893 and 897. The fluctuations in the relative abundance of all the species can be explained by the low total flux (3-12 #/cm^2*kyr), meaning that a small change in a species flux can have a large impact on the relative abundances. The mid Holocene appears to have unfavorable environmental conditions for Arctic and cold water species like *C. excavatum, I. norcrossi* and *C. reniforme*, indicating conditions were relatively warm. However, species associated with warm Atlantic water show a low presence, suggesting chilled bottom waters in the mid Holocene (Figure 19, Figure 20).

Looking at the high relative abundance (40-80%) of *M. barleeanus*, which would suggest a high availability of degraded organic material (Jennings, et al., 2011), this contradicts the decreasing flux, meaning another factor controlling *M. barleeanus* is dominating. This other factor could be a stable and higher clay content from 6900yr BP, around the same time TOC and the total flux stabilize on a lower value (Figure 20). The *M. barleeanus* flux has been relative stable since the early Holocene (8700yr BP), suggesting a change in the flux of other species rather than improved environmental conditions favorable for *M. barleeanus* (Figure 19).

The flux of most of the species in core 893 remain relative stable from 6900yr BP towards the present, even though the relative abundance changes. This can be due to the low total flux, meaning a small change in a species flux can give a significant change in relative abundance, as previously mentioned.

The relative abundance of *C. laevigata* declines and reaches a low point at 4500yr BP, suggesting a change in the physical environment or possibly a weakening in the inflow of Atlantic water indicating the start of a colder period. The decreasing total flux corresponds to the decline of the relative abundance and flux of *C. laevigata*, suggesting the increase in relative abundance of the other species is caused by the decrease of *C. laevigata* (Figure 19, Figure 20). The increase following the low point at 4500yr BP is similar for both *C. reniforme* and *C. laevigata*, while *M. barleeanus* and *L. lobatula* both show a decrease in the relative abundance, but an increase in the flux. This may suggest an environment with chilled Atlantic bottom water, allowing the opportunistic *C. reniforme* to increase its presence (Mackensen, et al., 1985; Elverhøi & Bomstad, 1980). At the very top of core 893, 4000yr BP, there is a slight increase in *Buccella* spp. and *Nonionella* spp., which might indicate a retreating summer sea-ice edge or a front (Figure 19, Figure 20).

It appears that the increase in *Buccella* spp. and *Nonionella* spp. flux can be traced northwards from core 893 to core 897, around 4000yr BP, where both species show a small general increase towards the late Holocene. This could suggest a northeastern movement of the Arctic Front from core 897 to core 893, as both *Buccella* spp. and *Nonionella* spp. are associated with the presence of a sea ice edge, Arctic Front and/or a marginal ice zone (MIZ), associated with high primary productivity (Polyak & Solheim, 1994; Hald & Steinsund, 1996; Jennings, et al., 2011). The *Buccella* spp. flux and relative abundance begins to decrease around 3500yr BP and reach 0% at 2500yr BP. *M. barleeanus* and *L. lobatula* both continue with the general decrease in relative abundance in core 897 (Figure 20). Around this time a possibility of dissolution of the calcareous tests are inferred by the high agglutinated flux relative to the calcareous flux (Figure 18), supporting the proximity of a sea ice edge or the Arctic Front (Steinsund & Hald, 1994).

From 4000yr BP to the end of the mid Holocene at 2500yr BP, episodes where *C. excavatum* and *C. reniforme* show a presence occur, suggesting some influence of cold, possibly Arctic, bottom water (Figure 20) over core 897. This partly supported by Slubowska-Woldengen et al. (2008) suggesting a cooling of the Barents Sea in the late middle Holocene, as they observed a dominance of *I. norcrossi* in the southeast Barents Sea and a dominance of *C. excavatum* and *C. reniforme* along the Svalbard and northern Barents Sea shelf. The dominance of *I. norcrossi* in the southeastern Barents Sea, found by Slubowska-Woldengen et al. (2008) is not present in core 897, where *I. norcrossi* show a low relative abundance of <2% (Figure 20). This could be because the cores used by Slubowska-Woldengen et al. (2008) are located further north.

At 3500yr BP, the total flux in core 897 show a positive peak, followed by a decline, similar to the decline spotted in core 893, about 7300yr BP. Due to the time difference of 3800yr it is not likely they reflect the same event causing the peak in total flux. The peak in core 897 ends at a low (4#/cm^2*ka) flux, about 2500yr BP, followed by a steady increase. In addition to this, the presence of *C. reniforme* and a brief appearance of *C. neoteretis* at 3500yr BP (Figure 20) may indicate chilled Atlantic water over core 897 between 4000yr BP and 2500yr BP. Risebrobakken et al. (2010) found similar results in the southwestern Barents Sea, closer to the Norwegian coast, where they observed a decline in total relative abundance of benthic Atlantic species between 4000yr BP and 2500yr BP. However, based on an increase in *A. weddellensis*, which is morphologically similar to *E. nipponica* (Saher, et al., 2012; Jennings, et al., 2011), they suggest a transition from chilled to less chilled Atlantic bottom water

throughout the period. The increase in *A. weddellensis* (*E. nipponica*) found by Risebrobakken et al. (2010) is not reflected in the occurrence of *E. nipponica* in this study.

M. barleeanus and *L. lobatula* are the dominant species in core 897 despite displaying a decrease in relative abundance towards the core top (Figure 20). This is likely due to changes in the physical environment, rather than the supply of nutrients, as *L. lobatula* thrives in coarse sediments, indicating strong hydrodynamic activity, and *M. barleeanus* prefers fine grained, calmer environments (Klitgaard-Kristensen, et al., 2002; Jennings, et al., 2011). This is supported by the relative stable flux of *M. barleeanu*s from 2700yr BP towards the late Holocene and the low (<2#/cm^2*ka), but changing flux of *L. lobatula*. The highest relative abundance of *M. barleeanus* occurs at the same point (2700yr BP) when the total calcareous flux is at a minimum, indicating a decrease for other species rather than a bloom of *M. barleeanus*, again supported by the relative stable *M. barleeanus* flux. This could suggest a weakening of the inflow of Atlantic water, bringing less organic material to the area, or the presence of sea ice, preventing primary production. Due to the lack of Arctic species and species associated with sea ice, it is not likely the area was covered by sea ice. In either case, the bottom water appears to have been cooler in the late part of the mid Holocene.

5.5 Late Holocene (2500-400yr BP)

The flux of *Buccella* spp. and *C. laevigata* begins to increase, starting at 2500yr BP, followed by an increase in *L. lobatula* flux, beginning about 1900yr BP, indicating stronger bottom currents and a gradual increase in bottom water temperature and salinity, possibly an increase in the strength of inflowing Atlantic water (Figure 19). Core 897 shows an increased sand concentration and sortable silt size from 1900yr BP to the top of the core (Figure 20). The flux is also at its lowest in core 897 at 1900yr BP, and the TOC value stabilizes. At 1400yr BP, *C. excavatum* appears again after being gone since 2500yr BP and *C. reniforme* begin to increase its presence. *I. norcrossi* also show increasing presence, indicating a shift to a colder environment, which could be caused by either a weakening of the inflow of Atlantic water or the proximity of a sea ice edge or possibly a combination. Given that species associated with colder bottom water, like *C. reniforme* and *I. norcrossi*, are dominating, it suggests chilled bottom water, possibly of Atlantic origin (Korsun & Hald, 1998; Mackensen, et al., 1985).

The general increase in the flux observed in both core 897 and 903 for the period from 2100yr BP towards 400yr BP, suggests an environment with more nutrients. The general increase of

Buccella spp., *I. norcrossi* and *Nonionella* spp. (Figure 19, Figure 20) suggest the presence of a sea ice edge or front close to core 897 and 903. Primary production close to a sea ice edge or front could explain the increasing TOC values (Jennings, et al., 2011; Hald & Steinsund, 1996).

The shift to a higher TOC content at 1700yr BP, in core 903, reflected in *C. excavatum, I. norcrossi* and *E. nipponica*. *C. excavatum* stabilize together with the TOC value at 1700yr BP and remain relative stable towards the core top. This can hint to colder conditions, which is supported by the same stabilizing trend for the relative abundance of *C. reniforme,* occurring a little earlier, about 1800yr BP. *E. nipponica,* almost disappear at this time, but show a gradual increase beginning at 1600yr BP towards the core top, indicating a shift to a warmer environment. However, the relative abundance of *E. nipponica* is low and due to the small size, it is susceptible to reworking and may be a result of that process (Hald & Steinsund, 1992; Saher, et al., 2012; Murray, et al., 1982). Even if *E.* nipponica is reworked, it still indicates a presence near the core location as it is not likely it is transported more than 100km before being redeposited. As the cold water species *C. excavatum, C. reniforme* and *I. norcrossi* show an increasing flux, generally higher than *E. nipponica,* it is more likely that *E. nipponica* occur as a result of reworking prior to 1600yr BP in the late Holocene. Around 1700yr BP the cold water species *C. excavatum, C. reniforme* and *I. norcrossi* are the dominating species.

The slight decrease of *C. excavatum* relative abundance from 1600yr BP towards the top of core 903 fits the slight overall increase in *C. reniforme,* from 1600yr BP to the core top, supporting a small increase in the inflow of Atlantic water. The beginning decrease of the relative abundance of *I. norcrossi* at 1700yr BP could indicate a retreating sea ice edge or front. This is supported by the relative stable high (around 14%) relative abundance of *C. excavatum* and *C. reniforme* as well as the steady increase in *E. nipponica* (from 1550yr BP). As little (<0.3g) IRD (Figure 9) were found during sieving, meaning it is not impossible that a few occasional melting icebergs have passed over the area. However, a front is more likely than a sea ice edge due to the small amount of IRD and the steady increase on *E. nipponica*. The incoming Atlantic water as a surface current would bring more organic material and increase the vertical flux of organic matter to the seafloor (Knies & Martinez, 2009), thus might explain the higher TOC values. This is supported by the lower relative abundance of cold water species such as *C. excavatum* and *C. reniforme* and a higher relative abundance of species associated with an sea ice edge or front, such as *Nonionella* Spp. (Jennings, et al.,

2011) prior to 1700yr BP. This suggests the presence of a front or sea ice edge at core 903 in the early part of the late Holocene. An alternate scenario could be that the Atlantic water was present and the Arctic Front moved to a position more proximal to the core location. However, as species associated with a front and presence of a sea ice edge show a higher presence in core 903 prior to the suggested advance of Atlantic water, it is believed a sea ice edge or front was present at core 903 prior to 1700yr BP, and pushed north by the Atlantic water at about 1700yr BP. The higher relative abundance of the cold water species *I. norcrossi*, prior to 1700yr BP, support this.

The upper and most recent part of core 897, 902 and 903, from 1500yr BP and younger, show peaks in the foraminiferal flux, suggesting episodes of enhanced productivity, although few changes in the species composition occur, the relative abundances display some change throughout this period. Together with a general coarsening of the grain sizes, this might suggest a more vigorous environment, possibly due to a stronger inflow of Atlantic water in the Barents See region (e.g. Groot et al. (2014), Slubowska et al. (2005) and Hass (2002)). Groot et al. (2014) observed similar peaks in the foraminiferal flux and small changes in the flux and abundance, as well as a coarsening of the grain sizes, in Kveithola trough for this period, supporting a more vigorous environment.

The increase of TOC and the flux of species associated with food availability, e.g. *M. barleeanus* and *Nonionella* spp. (Polyak & Solheim, 1994; Conradsen, et al., 1994), suggest increased food availability in northern part of Bjørnøyrenna (core 903, 902 and 897) for the last 1500 to 400 years (Figure 19). The increase in the flux of *C. excavatum, C. reniforme* and *I. norcrossi* at the same time as the increase in the species linked to food availability suggest the area to be influenced by seasonal sea ice, indicating a return of colder conditions and a reduction of the inflowing Atlantic water. It is also likely that a southward movement of the Arctic Front occurred, indicated by the increased flux of *Buccella* spp. and *Nonionella* spp. (Figure 19).

The peak in relative abundance of *C. neoteretis*, in core 903, correlates well with the period of lower sand and higher silt content between 1400yr BP and 1100yr BP. Throughout this period, *I. norcrossi* show a stable increasing presence, possibly indicating a temporarily return of a sea ice proximal environment (Jennings, et al., 2011). The increase in *C. neoteretis* could also indicate influence of transformed Atlantic bottom water (Wilson, et al., 2011). *M. barleeanus* show a lower relative abundance, but a stable flux, between 1500yr BP and

1400yr BP, suggesting an increase of the other species fluxes, like *L. lobatula* and *C. neoteretis* (Figure 19, Figure 20). The peak in the relative abundance and flux of *L. lobatula* might suggest a stronger bottom current. However, the low sand content for the period is not corresponding with stronger currents, inferred by *L. lobatula*, meaning a different factor is controlling the peak of *L. lobatula* for instance food availability.

The sand content in core 903 begins to increase at 1100yr BP and *L. lobatula* starts to disappear (Figure 19). As *L. lobatula* is associated with a turbulent, high-energy environment (Hald & Steinsund, 1996; Mackensen, et al., 1985), this suggests another controlling factor, for instance food availability, for the disappearance of the species around 1100yr BP. Simultaneously with the disappearance of *L. lobatula* and increase in the coarse grain size fraction, *M. barleeanus* show increasing presence even though it prefer fine-grained sediments (Hald & Steinsund, 1996; Jennings, et al., 2011; Mackensen, et al., 1985). This further supports food availability or another factor controlling *M. barleeanus*, *L. lobatula* and the rest of the species.

Both *L. lobatula* and *M. barleeanus* show a similar trend during the overlapping time span (1000-600yr BP) of core 897 and 902 (Figure 20), with a relative stable, slightly decreasing relative abundance of *M. barleeanus* and a general decline in *L. lobatula*, showing a similar declining pattern in both cores. The same is seen in the overlapping time span (1000-800yr BP) between core 902 and core 903 as well.

At 900yr BP, in core 902, the TOC content stabilize at a higher value (Figure 12), *C. laevigata* appears and *I. norcrossi* start to increase in abundance. *C. laevigata* disappear at 850yr BP while *I. norcrossi* continue to increase in both relative abundance and flux. This may suggest a cooling of the bottom water and possibly an advance of a sea ice edge or Arctic Front (Polyak & Solheim, 1994). The increase of *I. norcrossi* correspond with the clay content stabilizing at a lower value, as well as the sand content showing an increase towards the present. The general decrease of *L. lobatula* at 890yr BP does not seem to be controlled by the increase in sand content, thus suggesting food supply or another factor, such as a lowered salinity (Hald & Steinsund, 1996), controlling the decrease of *L. lobatula*.

Although the total calcareous flux has increased greatly from core 897 to core 902 (Figure 19), the general trend of the calcareous flux in core 902 is relative stable with the exception of an episode between 800yr BP and 700yr BP, with a peak in the calcareous flux (Figure 19).

The relatively steady relative abundance of *M. barleeanus* and *Nonionella* spp. and a decline in *L. lobatula* suggest the peak in total flux to affect all the considered species. Both TOC and the clay concentration show little change between 800yrBP and 700yr BP, but the sortable silt mean grain size and sand content are at a lower value during this time (Figure 12), suggesting a calmer environment. *C. excavatum* is the most affected species as the relative abundance of this species is increasing the most (Figure 19). This may suggest a pulse of cooler conditions entering the area from the north around 800yr BP. As the relative abundance to most of the other species show little response to the peak in total flux, and the steadily increasing relative abundance of *I. norcrossi*, it is likely that a pulse of cooler conditions from the north entered the southwestern Barents Sea.

Between 820yr BP and 730yr BP, in core 902, the total calcareous flux is high, although most of the species considered show an increasing flux around this time, *C. excavatum* and *L. lobatula* is the only species showing an increase in relative abundance (Figure 20). The relative abundance of *Buccella* spp., *M. barleeanus* and *Nonionella* spp. show a decline, and the flux of *M. barleeanus* and *Nonionella* spp. are decreasing, starting at 780yr BP towards the core top (Figure 20). Given the dominance of *C. excavatum*, *I. norcrossi* and *L. lobatula* during this time it suggests a colder period with higher hydrodynamic activity, as could be expected by a strong pulse of Arctic bottom water as previously inferred.

The high flux period between 820yr BP and 730yr BP, followed by an increase in sand content, support a continuation of the high energy environment, supported by the increase in *L. lobatula* towards the present. The brief introduction of *E. nipponica* at 650yr BP correspond to the increase in the coarser grain size fractions, and could occur as a result of higher currents, meaning they could be reworked (Hald & Steinsund, 1992; Saher, et al., 2012; Murray, et al., 1982). The relative abundance of *Buccella* spp. increase, starting at 730yr BP continuing to 400yr BP, possibly indicating a seasonal sea ice cover or Arctic Front in the northern part of the studied area in the southwestern Barents Sea (Polyak & Solheim, 1994; Hald & Steinsund, 1996).

Given the opportunistic nature of *C. excavatum* (Hald & Steinsund, 1996; Linke & Lutze, 1993) and the lower relative abundance of the species in core 902, it is believed that the environmental conditions have been relative stable throughout the timespan of core 902 (1000-600yr BP), with the exception of the proposed cold water period between 820yr BP and 730yr BP.

Although the total flux and TOC show a general increase up core in core 903, the increase does not seem to favor any particular species (Figure 19, Figure 20).

Between 700yr BP and 400yr BP the total flux is relative stable in core 902 and the relative abundance of *Buccella* spp. and *L. lobatula* increase. However, only the flux of *Buccella* spp. show an increase and as the species is often associated with a seasonal sea ice cover or front (Polyak & Solheim, 1994; Hald & Steinsund, 1996), it is not unlikely that a seasonal sea ice cover or front were present between 700yr BP and 400yr BP.

6 Conclusion

During the Late Glacial (15 500-14 900yr BP), the general trend is a warming of the bottom water, with increasing inflow of Atlantic water in the southern part of the study area (core 993). However, due to the possibility that parts of core 993 are reworked, care should be taken interpreting the results from the core.

During the early Holocene (10 900-7300yr BP) there was a general warming of the bottom water over core 893 in the southwestern Barents Sea, with higher current velocities and an increasing inflow of Atlantic water. This is inferred by the decreasing presence of the cold water species *C. excavatum, C. reniforme* and *I. Norcrossi* and increasing presence of warm water species such as *E. nipponica* and *C. laevigata* (Figure 20). At 9800yr BP strong bottom currents were present, inferred by a coarse sand fraction, no IRD and a peak in *L. lobatula*. The general warming trend found in this study is supported by the findings of Slubowska-Woldengen et al. (2008).

A cooling of the inflowing Atlantic water occurred during the mid Holocene (7300-2500yr BP), where the early parts are covered by core 893, and the late parts are covered by core 897, both located in the middle part of Bjørnøyrenna. This is inferred by a decrease in species associated with Atlantic water, such as *C. laevigata, C. neoteretis* and *E. nipponica* (Figure 20). However, the temperature did not drop enough for Arctic and cold water species like *C. excavatum* and *I. norcrossi* to occur. Atlantic water was still present during most of the mid Holocene, just colder than during the early Holocene. The decrease in Atlantic species and clay content suggest the mid Holocene to be a relative calm period. The first signs of a front occur at about 4000yr BP. Influence of Arctic water occurred in the late parts of the mid Holocene, indicating front proximal settings.

The start of the late Holocene (2500-400yr BP), covered by core 897, 902 and 903, remain chilled, inferred by *C. reniforme* and *I. norcrossi* (Figure 19, Figure 20), but at 1700yr BP the Arctic Front is pushed north. At 1500yr BP signs of a more vigorous environment is evident. It is likely that a marginal ice zone (MIZ) or Arctic Front is present in the northeastern part of the studied area for the early part of the late Holocene. A calmer environment occurs from 890yr BP with a pulse of Arctic water coming in from the north between 800-700yr BP, as inferred by *C. excavatum* among others (Figure 19, Figure 20). The latest part of the late

Holocene (700-400yr BP), covered by core 897 and 902, is a period with weaker currents and possibly a seasonal sea ice cover in the northern part of Bjørnøyrenna.

7 References

Aagaard-Sørensen, S., Husum, K., Hald, M. & Knies, J., 2010. Paleoceanographic development in the SW Barents Sea during the Late Weichselian-Early Holocene transition. *Quarternary Science Reviews 29 (25-26)*, pp. 3442-3456.

Allaby, M., 2013. *A dictionary of Geology and Earth Sciences.* 4. ed. s.l.:Oxford University Press.

Austin, W. E. N. & Sejrup, H. P., 1994. Recent shallow water benthic foraminifera from western Norway: ecology and paleoecological significance. *Cushman Foundation Special Publication 32*, pp. 103-125.

Blott, S. J., 2010. *GRADISTAT 8.0.* s.l.:s.n.

Board, W. E., 2016. *World Register of Marine Species (WoRMS).* [Online]
Available at: http://www.marinespecies.org/
[Accessed 2016].

Byrd polar research Center, 2001. *Foraminiferal research.* [Online]
Available at: http://research.bpcrc.osu.edu/geo/projects/foram/home.htm
[Accessed 16 December 2016].

Caralp, M. H., 1989. Abundance of Bulimina exilis and Melonis barleeanum: Relationship to the quality of marine organis matter. *Geo-Marine letters 9*, pp. 37-43.

Conradsen, K. et al., 1994. Recent Benthic foraminiferal distribution in the Kattagatt and Skagerrak, Scandinavia. *Cushman Foundation special publications, 32*, pp. 53-68.

Corliss, B. H., 1991. Morphology and microhabitat preferences of benthic foraminifera from the northwest Atlantic ocean. *Marine micropaleontology 17*, pp. 195-236.

Dessandier, P.-A.et al., 2015. Lateral and vertical distributions of living benthic foraminifera off the douro river (western Iberian margin): Impact of the organic matter quality. *marine microopaleontology 120*, pp. 31-45.

Dijkstra, N., Junttila, J. & Aagaard-Sørensen, S., 2016. Reconstructing pre-impact baseline conditions using benthic foraminifera in an area of increasing petroleum exploration activities. *Geophysical Reaserch Abstract 18*, pp. EGU2016-1253.

Dijkstra, N. et al., 2013. Baseline benthic foraminiferal assemblages and habitat conditions in a sub-Arctic region of increasing petroleum development. *Marine Environmental Research*, pp. 178-196.

Dijkstra, N. et al., 2015. Natural variability of benthic foraminiferal assemblages and metal concentrations during the last 150 years in the Ingøydjupet trough, SW Barents Sea. *Marine micropaeoltology 121*, pp. 16-31.

Eiriksson, J., Knudsen, K. L., Haflidason, H. & Heinemeyer, J., 2000. Chronology of late Holocene climatic events in the northern North Atlantic based on AMS 14C dates and tephra markers from the volcano Hekla, Iceland. *Journal of Quarternary Science 15 (6)*, pp. 573-580.

Eiriksson, J. et al., 2011. Coupling of paleoceanographic shifts and changes in marine reservoir ages off North Iceland through the last millenium. *Palaeogeography, paleoclimatology, paleoecology 302*, pp. 95-108.

Ellis, B. E. & Messina, A. R., 1940-1978. Catalogue of Foraminifera American Museum of Natural History, New York.

Elverhøi, A. & Bomstad, K., 1980. *Late Weichselian glacial and glaciomarine sedimentation in the western, central Barenst Sea,* Oslo: Norsk Polarinstitur.

Elverhøi, A., Hooke, R. L. & Solheim, A., 1998. Late Cenozoic erosion and sediment yield from the Svalbard-Barents Sea region: Implications for understanding erosion of glacierized basins. *Quarternary Science Reviews 17 (1)*, pp. 209-241.

Ercilla, G. & Casas, D., 2012. Submarine mass movements: Sedimentary Characterization and controlling factors. In: I. A. Dar, ed. *Earth Sciences.* s.l.:InTech, pp. 99-128.

Feyling-Hanssen, R. W., 1972. The Foraminifer Elphidium excavatum (Terquem) and its variant forms. *Micropaleontology 18 (3)*, pp. 337-354.

Gilbert, R., 1990. Rafting in glacimarine environments. *Geological society special publication, 53*, pp. 105-120.

Goddard, B. et al., 2016. Experimental setup and commisioning baseline study in search of time-variations in beta-decay half-lives. *Neuclear instruments and methods in physics reaserch section A: Accelerators, Spectrometers, Detectors and associated equipment, 812*, pp. 60-67.

Gothmann, A. M. et al., 2016. Cacium isotopes in scleractinian fossil corals since the Mesozoic: Implications for vital effects and biomineralization through time. *Earth and planetary science letters, 444*, pp. 205-214.

Groot, D. E., Aagaard-Sørensen, S. & Husum, K., 2014. Reconstruction of Atlantic water variability during the Holocene in the western Barents Sea. *Climate of the Past 10*, pp. 51-62.

Gutschick, R. C., 1986. Middle Ordovician agglutinated foraminifera including Reophax from the Miffin Formation, Platteville group of Illinois. *Journal of paleontology 60 (2)*, pp. 233-248.

Hald, M. & Steinsund, P. I., 1992. Distribution of surface sediment benthic foraminifera in the southwestern Barents Sea. *Journal of Foraminferal Research, v22, no4,* , pp. 347-362.

Hald, M. & Steinsund, P. I., 1996. Benthic foraminifera and carbonate dissolution in the surface sediments of the Barents and Kara Seas. In: R. Stein, I. Ivannov G, M. A. Levitan & K. Fahl, eds. *Surface-sediment composition and sedimentary processes in the central Arctic Ocean and along the Eurasian Continental Margin.* s.l.:Berichte zur Polarforschung, pp. 285-307.

Hald, M. et al., 1994. Recent and late quarternary distribution of Elphidium excavatum F. clavatum in Arctic seas. *Cushman Foundation Special Publications 32*, pp. 141-153.

Hald, M. & Vorren, T., 1984. Modern Holocene foraminifera and sediments on the continental shelf of Troms, North Norway. *Boreas, 13*, pp. 133-154.

Hald, M. & Vorren, T., 1987. Foraminiferal strathigraphy and environment of late Weichselian deposits on the continental shelf of Troms. northern Norway. *Mairone micropaleontology 12*, pp. 129-160.

Hass, C. H., 2002. A method to reduce the influence of ice-rafted debris on a grain size record from northern ram straight, Arctic Ocean. *Polar research, 21 (2)* , pp. 299-306.

Jennings, A., Andrews, J. & Wilson, L., 2011. Holocene environmental evolution of the SE Greenland shelf North and South of the Denmark Strait: Irminger and East Greenland current interactions. *Quarternary sciuence reviews* , pp. 980-998.

Jennings, A. E., Weiner, N. J., Helgadottir, G. & Andrews, J. T., 2004. Modern foraminiferal faunes of the southwestern to northern Iceland shelf: oceanographic and environmental controls. *Journal of foraminiferal research 34*, pp. 180-207.

Junttila, J., Aagaars-Sørensen, S., Husum, K. & Hald, M., 2010. Late glacial-Holocene clay minerals elucidating glacial history in the SW Barents Sea. *Marine Geology 276*, pp. 71-85.

Junttila, J., Carrol, J., Husum, K. & Dijkstra, N., 2014. Sediment transport and deposition in the Ingøydjupet trough, SW Barents Sea. *Continental shelf research 76*, pp. 53-63.

Junttila, J., Carroll, J. & Dijkstra, N., 2015. Variability of present and past PAH (polyaromatic hydrocarbons) concentrations in sediments of the SW Barents Sea. *Norwegian journal of geology, 95* , pp. 191-210.

Kartverket, n.d. *Norgeskart.* [Online]
Available at:
https://norgeskart.no/geoportal/#3/995102/8314071/l/wms/[http://maps.imr.no/geoserver/ows]/+Arctic_background/+barents_sea_currents
[Accessed Desember 2016].

Kennedy, M. J., Peaver, D. R. & Hill, R. J., 2002. Mineral surface control of organic carbon in black shale. *Science 295*, pp. 657-660.

Khusid, T. K. & Korsum, S. A., 1996. Modern benthic foraminiferal assemblages in the Kara Sea. In: R. Stein, G. I. Ivanov, M. A. Levitan & K. Fahl, eds. *Surface-sediment composition and sedimentary processes in the central Arctic Ocean and aling the Euasian continental margin.* s.l.:Ber. Polarforsch. 212, pp. 308-314.

King, E. L. et al., 2014. Contour current driven continental slope-situated sandwaves with effects from secondary current processes on the Barents Sea margin offshore Norway. *Marine Geology 353*, pp. 108-127.

Klitgaard-Kristensen, D., Sejrup, H. P. & Haflidason, H., 2002. Distribution of recent calcareous benthic foraminifera inthe northern North Sea and relation to the environment. *Polar research 21 (2)*, pp. 275-282.

Klitgaard-Kristensen, D., Sejrup, H. P. & Haflidason, H., 2001. The last 18 kyr fluctuations in Norwegian Sea surface conditions and implications for the magnitude of climatc change: evidence from the North Sea. *Paleoceanography 16 (5)*, pp. 455-467.

Knies, J. & Martinez, P., 2009. Organic matter sedimentation iin the western Barents Sea region: Terrestrial and marine contribution based on isotopic composition and organic nitrogen content. *Norwegian journal of geology, 89*, pp. 79-89.

Knudsen, K. L. & Ausin, W. E. N., 1996. Late Glacial Foraminifera. *Geological society, London, Special Publications 111*, pp. 7-10.

Korsun, S. & Hald, M., 1998. Modern Benthic foraminifera off Novaya Zemlya tidewater Glaciers, Russian Arctic. *Arctic and Alpine Research 30 (1)*, pp. 61-77.

Lagoe, M. B., Eyles, C. H. & Eyles, N., 1994. Foraminiferal biofacies and paleoenvironments in a pliocene megachannel of the glaciomarine Yakatage formation, gulf of Alaska. *Cushman Foundations Spacial Publication 32*, pp. 127-139.

Lambeck, K., 1996. Limits on the areal extend of the Barents Sea ice sheet in Late Weichselian time. *Global planetary change 12*, pp. 41-51.

Landvik, J. Y. et al., 1998. The last glacial maximum of Svalbard and the Barents Sea area: ice sheet extent and configuration. *Quarternary science reviews 17*, pp. 43-75.

Linke, P. & Lutze, G. F., 1993. Microhabitat preferences of benthic foraminifera - a static concept or a dynamic adaption to optimize food aquisition?. *Marine micropaleontoogy 20*, pp. 215-234.

Loeblich, A. R. & Tappan, H., 1987. *Foraminiferal Genera and Their Classification.* New York: Van Nostrand Reinhold Co.

Loeng, H., 1991. Features of the physical oceanographic conditions of the Barents Sea. *Polar research, 10*, pp. 5-18.

Mackensen, A. & Hald, M., 1988. Cassidulina teretis Tappan and C. laevigata D'orbigny: their modern and late quarternary distribution in northern seas. *Journal of foraminiferal research 18 (1)*, pp. 16-24.

Mackensen, A., Sejrup, H. P. & Jansen, E., 1985. The distribution of living benthic foraminifera on the continental slope and rise off southwest Norway. *Marine micropaleontology 9*, pp. 275-306.

Mangerud, J. et al., 2006. Marine 14C reservoir ages for 19th century whales and molluscs from the North Atlantic. *Quarternary Science Reviews, 25*, pp. 3228-3245.

Mangerud, J. & Gulliksen, S., 1975. Apparent radiocarbon ages of recent marine shells from Norwy, Spitsbergen and Arctic Canada. *Quarternary Research 5*, pp. 263-273.

Mangerud, J. et al., 2004. Ice-dammed lakes and rerouting of the drainage of northern Eurasia during the Last Glaciation. *Quarternary science reviews 23*, pp. 1313-1332.

Montfort, P. D. D., 1808. *Conchyliologie systématique, et classification méthodique des coquilles.* 1. ed. Paris: Schoell, Fraedaeric.

Mudie, P. J., Keen, C. E., Hardy, I. A. & Vilks, G., 1984. Multivariate analysis and quantitative paleoecology of benthic foraminifera in surface and late Quarternary shelf sediments, northern Canada. *Marine Micropaleontology 8*, pp. 283-313.

Murray, J. W., 2006. *Ecology and applications of Banthic foraminifera.* s.l.:Cambridge university press.

Murray, J. W., Sturrock, S. & Weston, J., 1982. Suspended load transport of foraminiferal tests in a tide- and wave-swept sea. *Journal of Foraminiferal Research 12 (1)*, pp. 51-65.

Patterson, R. T. & Fishbein, A., 1989. Re- examination of the statistical methods used to determen the number of point counts needed for micropaleontological quantitative research. *J. Paleont, 63(2)*, pp. 245-248.

Polyak, L. et al., 2002. Benthic foraminiferal assamblages from the southern Kara Sea, A river-influenced Arctic marine environment. *Journal of foraminiferal research 32*, pp. 252-273.

Polyak, L. & Mikhailov, V., 1996. Post-glacial envireonments of the southeastern Barents Sea: foraminiferal evidence. *geological society special publications 111*, pp. 323-337.

Polyak, L. & Solheim, A., 1994. Late- and post glacial environments of the northern Barents Sea west of Franz Josef Land. *Polar Research 13 (2)*, pp. 197-207.

Purser, K. H. & Litherland, A. E., 1990. The elimination of cherge-changing backgrounds in an AMS radiocarbon system. *Nuclear instruments and Methods in Physics Reaserch, B52,* pp. 424-427.

Rahmstorf, S., 2006. Thermohaline Ocean circulation. In: *Encyclopedia of Quarternary Sciences.* Amsterdam: Elsevier.

Rasmussen, T. L. et al., 2007. Paleoceanographic evolution of the SW Svalbard margin (76°N) since 20,000 14C yr BP. *Qouarternary research 67,* pp. 100-114.

Risebrobakken, B. et al., 2010. Climate and oceanographic variability in the SW Barents Sea during the Holocene. *The Holocene,* pp. 1-13.

Ruther, D. C. et al., 2011. Seismic architecture and sedimentology of a major grounding zone system deposited by the Bjørnøya Ice Stream during Late Weichselian deglaciation. *Quarternary Science Reviwes, 30* , pp. 2776-2792.

Saher, M. et al., 2012. Changes in distribution of calcareous benthic foraminifera in the central Barents Sea between the periods 1965-1992 and 2005-2006. *Global and Planetary Change 98-99,* pp. 81-96.

Saher, M. et al., 2009. Benthic foraminifera assemblages in the Central Barents Sea: an evaluation of the effect of combining live and todal fauna studies in tracking environmental change. *Norwegian Journal og Geology 89,* pp. 149-161.

Schröder, C. J., Scott, D. B. & Medioli, F. S., 1987. Can smaller benthic foraminfera be ignored in paleoenvironmental analyses?. *Journal of foraminiferal research, 17 (2),* pp. 101-105.

Seidenkrantz, M.-S., 1995. Cassidulina teretis Tappan and Cassidulina neoteretis new species (Foreminifera): stratigraphic markers for deep sea and outer shelf areas. *Micropaleontology 14 (2),* pp. 145-157.

Sejrup, H.-P.et al., 1981. Benthonic Foraminifera in surface samples from the Norwegian continental margin between 62°N and 65°N. *Journal of foraminiferal research 11 (4),* pp. 277-295.

Sejrup, H. P., Birks, H. J. B., Klitgaard, K. D. & Madsen, H., 2004. Bnthonic foraminiferal distributions and quantitative transfer functions for the northwest European continental margin. *Marine Micropaleontology 53* , pp. 197-226.

Slobuwska-Woldengen, M. et al., 2007. Advection of Atlantic Water to the western and northern Svalbard shelf since 17,500 cal yr BP. *Quarternary Science Reviews 26,* pp. 463-478.

Slubowska, M. A., Koc, N., Rasmussen, T. L. & Klitgaard-Kristensen, D., 2005. Changes in the flow of Atlantic water into the Arctic Ocean since the last degalciation: Evidence from the northern Svalbard continental margin, 80°N. *Paleoceanograohy 20*, pp. 1-15.

Slubowska-Woldengen, M. et al., 2008. Time-Slice reconstructions of ocean circulation changes on the continental shelf in the Nordic and Barents Seas during the last 16,000 cal yr B.P.. *Quarternary Science Reviewes, 27*, pp. 1476-1492.

Smedsrud, L. H. et al., 2013. The role of the Barents Sea in the Arctic climate system. *Reviews of Geophysics 51 (3)*, pp. 415-449.

Steinsund, P. I. & Hald, M., 1994. Recent calcium carbonate dissolution in the Barents Sea: Paleoceanographic applications. *Marine Geology 117*, pp. 303-316.

Struck, U., 1995. Stepwise postglacial migration of benthic foraminifera into the abyssal northeastern Norwegian Sea. *Marine Micropaleontology 26*, pp. 207-213.

Stuvier, M., Pearson, G. & Brasiunaz, T., 1986. Radiocarbon age calibration of marine samples back to 9000 cal yr BP. *Radiocarbon, 28 (2B)*, pp. 980-1021.

Tappan, H., 1951. Northern Alaska index Foraminifera. *Contributions from the Cushman Foundation for Foraminiferal Research 2 (1)*, pp. 1-8.

Usami, K., Ohi, T., Hasegava, S. & Ikehara, K., 2013. Foraminiferal records of bottom-water oxygenation and surface-water productivity in the southern Japan Sea during 160-15 ka: Associations with insolation changes. *Marine micropaleontology 101*, pp. 10-27.

Vorren, T. O., Hald, M. & Lebsbye, E., 1988a. Late Cenozoic environments in the Barents Sea. *Paleoceanography 3 (5)*, pp. 601-612.

Vorren, T. O. et al., 1988b. The last deglaciation (20,000 to 11,000 BP) on Andøya, northern Norway. *Boreas 17*, pp. 41-77.

Wilson, L. J., Hald, M. & Godtliebsen, F., 2011. Foraminiferal faunal evidence of twentieth-century Barents Sea warming. *The Holocene 21 (4)*, pp. 527-537.

Wollenburg, J. E. & Mackensen, A., 1998. Living benthic foraminifers from the central Arctic Ocean: faunal composition, standing stock and diversity. *Marine micropaleontology 34*, pp. 153-185.

Appendix 1: Species list

Adercotryma glomerata
Armorella spp.
Cribrostromoides spp.
Rahbdamina spp.
Reophax spp.
Trochammina spp.
Astronion Gallowayi
Bolivina spp.
Bolivina pseudopunkta
Buccella spp.
Bulimina spp.
Cassidulina laevigata
Cassidulina neoteretris
Cassidulina obtusa
Cassidulina spp.
Cornuspira spp.
Cribroelphidium albiumbilicatum
Cribroelphidium excavatum
Dentalina spp.
Eilohedra nipponica
Elphidae spp.
Elphidium bartletti
Elphidium incertum
Epistominella spp.
Fissurina spp.
Glandulina ovula
Glandulina spp.
Globobulimina auriculata
Globobulimina spp.
Haynelina balthica
Haynesina depressula
Haynesina germanica
Haynesina orbiculare
Islandiella helenae
Islandiella norcrossi
Islandiella spp.
Lagena spp.
Lenticulina spp.
Lenticulina Thalmanni
Lobatula lobatula
Melonis barleanus
Miliolinella spp.
Nonionella auricular
Nonionella labradorica
Nonionella turgida
Oolina spp.
Pullenia bulloides
Pullenia spp.
Pyrgo Wiliamsoni
Quinqueloculina seminula
Quinqueloculina spp.
Robertinoides spp.
Sigmoilina spp.
Stainforthia concava
Stainforthia feylingi
Stainforthia loeblichi
Stainforthia spp.
Stainforthia fussiformis
Trifarina angulosa
Trifarina fluens
Triloculina spp.
Valvulina spp.

In total 62 species were identified, where six are agglutinated and 56 are calcareous.

Appendix 2: Sample Interval

core	depth interval
HH12-893 MCD	20-21
	21-22
	22-23
	23-24
	24-25
	25-26
	26-27
	27-28
	28-29
	29-30
	30-31
	31-32
	32-33
	33-34
	34-35
	35-36
	36-37
	37-38
	38-39
	39-40
	40-41
HH12-897 MCA	20-21
	21-22
	22-23
	23-24
	24-25
	25-26
	26-27
	27-28
	28-29
	29-30
	30-31
	31-32
	32-33
	33-34
	34-35
	35-36
	36-37
	37-38
	38-39
	39-40

core	depth interval
HH12-902 MCC	20-21
	21-22
	22-23
	23-24
	24-25
	25-26
	26-27
	27-28
	28-29
	29-30
	30-31
	31-32
	32-33
	33-34
	34-35
	35-36
	36-37
	37-38
	38-39
	39-40
	40-41
	41-42
	42-43
	43-44
HH12-903 MCC	20-21
	21-22
	22-23
	23-24
	24-25
	25-26
	26-27
	27-28
	28-29
	29-30
	30-31
	31-32
	32-33
	33-34
	34-35
	35-36
	36-37
	37-38
	38-39
	39-40
	40-41
	41-42
	42-43
	43-44
	44-45

core	depth interval
IG15-1-993-MCC	20-21
	21-22
	22-23
	23-24
	24-25
	25-26
	26-27
	27-28
	28-29,5
	29,5-31